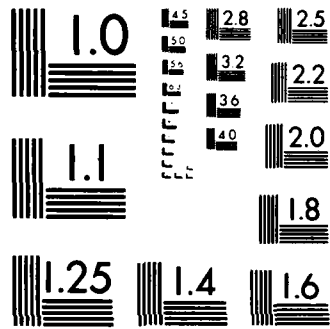




\_\_\_\_\_

\_\_\_\_\_



MICROCOPY RESOLUTION TEST CHART  
NATIONAL BUREAU OF STANDARDS-1963-A

JR+E 8526

AD-A155 330

EFFECTS OF WEAK INTERFACES ON THERMOSTRUCTURAL BEHAVIOR  
OF CARBON-CARBON COMPOSITES

Annual Report  
Contract N00014-82-C-0405

by  
Julius Jortner

Submitted by  
Jortner Research & Engineering, Inc.  
P. O. Box 2825  
Costa Mesa, CA 92628

to

OFFICE OF NAVAL RESEARCH  
800 North Quincy Street  
Arlington, VA 22217

March 1985



JUN 21 1985

A

Approved for Public Release; Distribution Unlimited

85 6 3 155

DTIC FILE COPY

SECURITY CLASSIFICATION OF THIS PAGE (When Data Entered)

REPORT DOCUMENTATION PAGE		READ INSTRUCTIONS BEFORE COMPLETING FORM
1. REPORT NUMBER	2. GOVT ACCESSION NO. AD-A155533C	3. RECIPIENT'S CATALOG NUMBER
4. TITLE (and Subtitle) EFFECTS OF WEAK INTERFACES ON THERMOSTRUCTURAL BEHAVIOR OF CARBON-CARBON COMPOSITES		5. TYPE OF REPORT & PERIOD COVERED Annual Report 1 Dec 84 to 31 Mar 85
		6. PERFORMING ORG. REPORT NUMBER JR+E 8526
7. AUTHOR(s) Julius Jortner		8. CONTRACT OR GRANT NUMBER(s) N00014-82-C-0405
9. PERFORMING ORGANIZATION NAME AND ADDRESS Jortner Research & Engineering, Inc. P. O. Box 2825 Costa Mesa, CA 92628		10. PROGRAM ELEMENT, PROJECT, TASK AREA & WORK UNIT NUMBERS NR 039-235
11. CONTROLLING OFFICE NAME AND ADDRESS Office of Naval Research 800 N. Quincy Street Arlington, VA 22217		12. REPORT DATE 31 March 1985
		13. NUMBER OF PAGES viii + 54
14. MONITORING AGENCY NAME & ADDRESS (If different from Controlling Office)		15. SECURITY CLASS. (of this report) UNCLASSIFIED
		15a. DECLASSIFICATION/DOWNGRADING SCHEDULE
16. DISTRIBUTION STATEMENT (of this Report)  Approved for Public Release; Distribution Unlimited		
17. DISTRIBUTION STATEMENT (of the abstract entered in Block 20, if different from Report)		
18. SUPPLEMENTARY NOTES		
19. KEY WORDS (Continue on reverse side if necessary and identify by block number)  Composite materials                      Mechanical properties Carbon-Carbon composites              Thermal properties Micromechanics                              Stress-strain behavior		
20. ABSTRACT (Continue on reverse side if necessary and identify by block number) Continuing research into mechanical and thermal behavior of carbon-carbon composites is described. Results presented include a theory for tensile fracture of yarn-bundles in which the fiber-matrix interface is weak, a mini-mechanical shear-lag analysis of thermal expansion of 3D carbon-carbons showing that interconstituent slippage has large effects on thermal expansion test data, a discussion of the role of radial yarns during heat treatment of cylindrical 3D billets, and an initial analysis of the effects on constitutive behavior of strain-induced microscale rotations of fibers.		

DD FORM 1473  
1 JAN 73

EDITION OF 1 NOV 65 IS OBSOLETE

UNCLASSIFIED

SECURITY CLASSIFICATION OF THIS PAGE (When Data Entered)



CONTENTS

Report Documentation Page, DD1473..... i

Foreword..... iii

List of Illustrations..... vii

Chapter 1. Introduction..... 1

Chapter 2. On the Role of Radial Yarns in Heat-Treatment of 3D  
Cylindrical Carbon-Carbon Billets..... 3

Chapter 3. Effects of Strain-Induced Material Rotations on  
Stress-Strain Behavior..... 9

Appendix A. A Model for Tensile Fracture of Carbon-Carbon  
Composite Fiber Bundles..... 19

Appendix B. Effects of Shear Lag on Thermal Expansion of 3D  
Carbon-Carbon Composites..... 33

Appendix C. Effects of Weak Interfaces on Thermal Expansion of 3D  
Carbon-Carbon Composites..... 49

References..... 53

## LIST OF ILLUSTRATIONS

Figure	Page
1. Schematic of stress distribution in a uniformly heated cylindrically orthotropic cylinder with radial thermal expansion greater than hoop thermal expansion.....	5
2. Effects of strain on texture angle.....	10
3. Illustrating the effect of a structure's geometry and loading conditions on the sensitivity of fiber orientation to shear strain.....	10
4. Illustrating the factor $\phi$ and dependence of microscale rotation on coordinate definitions.....	11
5. Effects of current shear strain, and ratio of applied shear strain increment to applied axial strain increment, on slopes of stress-strain responses in combined shear-compression loading. Top graph shows slope of compressive stress-strain curve. Lower graph shows slope of shear stress-strain curve.....	13
6. Effects of current fiber tilt angle, and ratio of applied shear stress increment to applied axial stress increment, on slopes of stress-strain responses in combined shear-compression loading. Top graph shows slope of compressive stress-strain curve. Lower graph shows slope of shear stress-strain curve.....	17
7. Effects of tilt angle on Young's modulus in uniaxial loading.....	18

PREVIOUS PAGE  
IS BLANK



## Chapter 1

## INTRODUCTION

The research described in this interim report is a continuation of the studies reported previously (Ref. 1-3). The main goal continues to be understanding the thermal and mechanical behavior of composites that contain microstructural cracks as a consequence of the heat treatments involved in their fabrication. Although the research is directed especially toward carbon-carbon composites, the findings may be applicable in principle to the broader category of composites with ceramic matrices.

The matrix phase and the several types of interconstituent interfaces in carbon-carbons are weak because of the microcracks and, also, because of factors related to the anisotropy of graphite. These weaknesses do not destroy the technological value of the composites, which relies mainly on the high strength of the fibers and the thermal-stress resistance of the composite. However, the weakness of the interfaces does have substantial effects on thermo-mechanical behavior.

When the interface between fiber and matrix in a yarn bundle gives way, the tensile strength of the composite is affected. The paper in Appendix A proposes a theoretical model of tensile fracture for yarn bundles with weak fiber-matrix interfaces. Thermal expansion of the composite also may be substantially affected by slip at interfaces between yarn bundles and the rest of the composite; the paper in Appendix B provides a theoretical analysis of thermal expansion tests using a shear lag model to account for interconstituent slippage. The paper in Appendix C is a condensed version of Appendix B.

Effects of interfacial behavior on tensile strength and on thermal expansion appear relevant to the occurrence of fractures in cylindrical billets during processing heat treatments. In particular, interfacial behavior appears to determine the extent to which radial yarn bundles can be relied on to prevent billet fractures. Chapter 2 is a discussion of some of the issues involved, which are under continuing study here and at UCLA (Ref. 15).

Chapter 3 discusses a peculiarity of stress-strain behavior of unidirectional and 3D carbon-carbon composites under multiaxial stresses. The extremely low values of shear modulus, obtained in carbon-carbons as a result of the weak interfaces, imply that adequate constitutive relations must account for strain-induced microscale rotations of the reinforcing fibers. That is, explaining the behavior of carbon-carbons, even at small strains, requires concepts borrowed from finite-strain elasticity theory.



Other activities during the last year, for which reporting is deferred, include:

- a) development of a computer code to estimate stresses in 3D cylinders during heat treatment, with accounting for shear lag at the radial bundles,
- b) development of a theoretical criterion for delamination in 2D carbon-carbons under combined stresses,
- c) construction of a "tele-microscope" to enable high-resolution recordings of microstructural changes at the surfaces of mechanical test specimens during test, and
- d) planning of experiments to further study the effect of notches on torsional behavior (cf, Ref. 3).

In addition to the papers reproduced in the Appendices, other publications or presentations deriving from this research project during the last year include a lecture on carbon-carbons to the 1984 Gordon Conference on Composites (Santa Barbara, Jan. 1984), participation in the ONR Workshop on Research Priorities (Ref. 4), a lecture to the AFRPL Carbon-Carbon Composites Workshop (Ref. 5), and a talk to the American Ceramic Society (Ref. 6).

## Chapter 2

ON THE ROLE OF RADIAL YARNS DURING HEAT-TREATMENT OF 3D CYLINDRICAL  
CARBON-CARBON BILLETS

Computer codes such as DCAP, BOUND, and MIPAC (Ref. 7, 8, and 9) can estimate the stresses in the mini-constituents (yarn bundles and matrix pockets) of a 3D composite, during heating and stressing of the composite. These minimechanical codes, when used with a general finite element program such as SAAS (Ref. 10), comprise an ability to do linear elastic analyses of a carbon-carbon structure, modeling the 3D composite as a continuum composed of yarn bundles and matrix regions that are bonded to each other. When such tools are applied to analysis of stresses during heat treatment of specific cylindrical billets of 3D carbon-carbon (as in Ref. 11, 12, and 13), the results always have shown that the radial yarn bundles are more highly stressed than are the circumferential (hoop) bundles (Ref. 12, for example).

The brief first-order analysis given below proves this result is generally true for 3D billets reinforced in a cylindrically orthogonal manner, whenever the composite's thermal expansion in the radial direction exceeds its thermal expansion in the hoop direction. It has been shown (eg, Ref. 1) that this inequality of thermal expansions occurs when, as is usually the case, the volume fraction of radial fibers is less than that of the hoop fibers (if the same fiber is used in the radial and hoop directions).

The analysis is intended to provide results that are simple enough to guide one's intuition, at the expense of some rigorous detail, more or less in the spirit of the work of Sines and his co-workers (Ref. 14 and 15). After proving that the radial yarns experience higher stresses than do the hoop yarns, we discuss some implications as background for our continuing analytical study, to be reported in the next annual report, of the role of the radial yarns during heat treatment of cylindrical billets.

A FIRST-ORDER APPROXIMATION OF STRAINS IN RADIAL BUNDLES DURING HEAT  
TREATMENT OF 3D CYLINDRICAL BILLETS

Consider a cylinder of inner radius  $a$  and outer radius  $b$ , made of a composite material for which the coefficient of thermal expansion in the radial direction,  $\alpha_r$ , is larger than the circumferential expansion coefficient,  $\alpha_\theta$ . On heating from the stress-free temperature by applying a uniform temperature increase,  $\Delta T$ , the cylinder will experience thermal stresses that vary with radial position as shown schematically in Figure 1.

The approximate analysis begins by noting that the stresses induced by heating must be self-equilibrating; therefore, the composite's tensile hoop stress at the outer radius is approximately equal to the compressive hoop stress at the inner radius:

$$\left({}^c\sigma_\theta\right)_{r=b} \cong -\left({}^c\sigma_\theta\right)_{r=a} \quad (1)$$

if the thickness of the cylinder is not too large relative to its radius.

The cylinder is a 3D composite of cylindrical orthotropy, with fiber bundles oriented in the radial, axial, and circumferential directions. We simplify by assuming the composite stiffnesses do not vary with radial position, and that the Poisson's ratios of the composite are negligibly small in the  $r, z, \theta$  coordinate frame. Then Eq 1 implies:

$$\left({}^c\epsilon_\theta\right)_{r=b} \cong -\left({}^c\epsilon_\theta\right)_{r=a} \quad (2)$$

where  ${}^c\epsilon$  denotes mechanical strain in the composite.

On the average, at any location, the total strain in a fiber bundle will equal the composite's total strain in the same direction. The total strain is the sum of the mechanical strain and the thermal strain:

$$e = \epsilon + \alpha \Delta T \quad (3)$$

Therefore:

$${}^B\epsilon_j + {}^B\alpha \Delta T = {}^c\epsilon_j + {}^c\alpha_j \Delta T \quad (3a)$$

and

$${}^B\epsilon_j = {}^c\epsilon_j + \left({}^c\alpha_j - {}^B\alpha\right) \Delta T = {}^c\epsilon_j - {}^B\alpha \Delta T \quad (4)$$

where  ${}^B\alpha$  is the longitudinal thermal expansion coefficient of the bundles, assumed the same for all three directions, and  $\Delta T$  is the temperature rise from a stress-free temperature. Here, the superscripts B and C refer to bundle and composite, respectively, and the subscript j can refer to the  $r, z, \theta$  directions in the cylinder.

The average total radial strain in the composite is related to the inner and outer radii before and after heating:

$$\overline{{}^c\epsilon_r} = \frac{(b'-a') - (b-a)}{b-a} \quad (5)$$

where the radii after heating are:

$$b' = b \left(1 + {}^c\epsilon_\theta^* + {}^c\alpha_\theta \Delta T\right) \quad (6)$$

$$a' \cong a \left(1 - {}^c\epsilon_\theta^* + {}^c\alpha_\theta \Delta T\right) \quad (7)$$

and  ${}^c\epsilon_{\theta}^*$  is the peak circumferential mechanical strain in the composite (which occurs at the outer radius). Then, by substituting Eq 6 and 7 in Eq 5:

$$\overline{{}^c\epsilon_r} \cong {}^c\epsilon_{\theta}^* \left( \frac{b+a}{b-a} \right) + {}^c\alpha_{\theta} \Delta T \quad (8)$$

From Eq 8 and 4, the average mechanical strain in the radial bundles is:

$$\overline{{}^B\epsilon_r} \cong {}^c\epsilon_{\theta}^* \left( \frac{b+a}{b-a} \right) + ({}^c\alpha_{\theta} - {}^B\alpha) \Delta T \quad (9)$$

From Eq 4, the maximum mechanical strain in the circumferential bundles is:

$${}^B\epsilon_{\theta}^* = {}^c\epsilon_{\theta}^* + ({}^c\alpha_{\theta} - {}^B\alpha) \Delta T \quad (10)$$

The ratio of the average radial-bundle mechanical strain to the maximum circumferential-bundle mechanical strain is therefore:

$$\frac{\overline{{}^B\epsilon_r}}{{}^B\epsilon_{\theta}^*} = \frac{{}^c\epsilon_{\theta}^* \left( \frac{b+a}{b-a} \right) + ({}^c\alpha_{\theta} - {}^B\alpha) \Delta T}{{}^c\epsilon_{\theta}^* + ({}^c\alpha_{\theta} - {}^B\alpha) \Delta T} \quad (11)$$

which is greater than one because  $\frac{b+a}{b-a}$  is greater than one.

In other words, by subtracting Eq 10 from Eq 9, we find the difference between  $\overline{{}^B\epsilon_r}$  and  ${}^c\epsilon_{\theta}^*$  is always positive:

$$\overline{{}^B\epsilon_r} - {}^c\epsilon_{\theta}^* = {}^c\epsilon_{\theta}^* \left( \frac{2a}{b-a} \right) \quad (12)$$

To find the maximum tensile mechanical strain in the radial bundles, we note that the composite's radial stress is compressive (Figure 1). The composite's maximum radial mechanical strain therefore

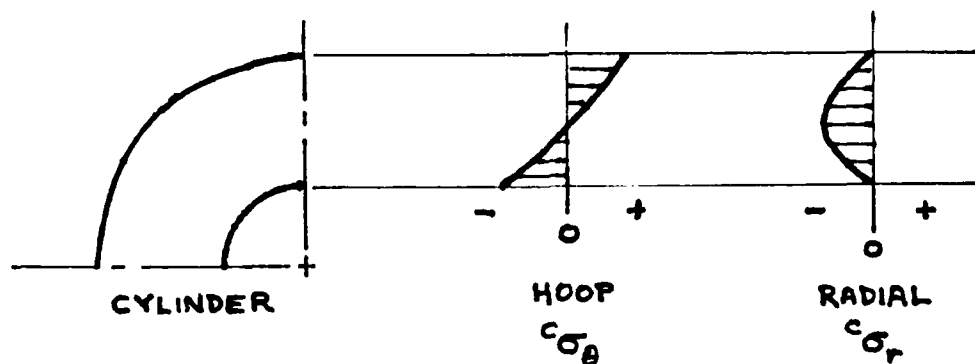


Figure 1. Schematic of stress distribution in a uniformly heated cylindrically orthotropic cylinder with radial thermal expansion greater than hoop thermal expansion.

occurs at the inner or outer radii, and is approximately zero (assuming, again, that Poisson's ratios are of negligible importance). Thus, from Eq 4, the maximum mechanical strain in the radial bundles is:

$${}^B\epsilon_r^* \cong ({}^C\alpha_r - {}^B\alpha) \Delta T \quad (13)$$

Comparing Eq 13 and Eq 10 gives the relationship of maximum mechanical strains in the radial and circumferential bundles:

$$\frac{{}^B\epsilon_r^*}{{}^B\epsilon_\theta^*} \cong \frac{({}^C\alpha_r - {}^B\alpha) \Delta T}{{}^C\epsilon_\theta^* + ({}^C\alpha_\theta - {}^B\alpha) \Delta T} \quad (14)$$

and

$${}^B\epsilon_r^* - {}^B\epsilon_\theta^* \cong ({}^C\alpha_r - {}^C\alpha_\theta) \Delta T - {}^C\epsilon_\theta^* \quad (15)$$

From equation 15, and the previously established fact that  $\overline{{}^B\epsilon_r} > {}^B\epsilon_\theta^*$  (Eq 12), we note that:

$$({}^C\alpha_r - {}^C\alpha_\theta) \Delta T > {}^C\epsilon_\theta^* \quad (16)$$

from which it appears that the thermal expansion strains  ${}^C\alpha\Delta T$  are of the same order as, or larger than,  ${}^C\epsilon_\theta^*$ .

From the fact that the composite's average radial mechanical strain is negative (Fig. 1), another inequality is obtained:

$$({}^C\alpha_r - {}^C\alpha_\theta) \Delta T > {}^C\epsilon_\theta^* \left( \frac{b+a}{b-a} \right) \quad (17)$$

which shows that the factor  $\frac{{}^C\epsilon_\theta^*}{b-a}$  is bounded. That is,  ${}^C\epsilon_\theta^*$  approaches zero as the cylinder thickness approaches zero; at the same time, the bundle mechanical strains approach:

$${}^B\epsilon_r^* \rightarrow ({}^C\alpha_r - {}^B\alpha) \Delta T \quad (18)$$

$${}^B\epsilon_\theta^* \rightarrow ({}^C\alpha_\theta - {}^B\alpha) \Delta T \quad (19)$$

which are the values that apply to a cartesian 3D composite.

#### REMARKS

This analysis shows that the mechanical strains in the radial bundles are tensile on average, in spite of the fact that the composite's stress in the radial direction is compressive. Also, we conclude that the average radial-bundle stress is greater than the maximum hoop-bundle stress (Eq 12).\*

\* Although they reach the same conclusion, Quan et al rely on an equation (Eq I-8, page 9 of Ref. 15) that oversimplifies by assuming incorrectly that the thermal strains are small relative to elastic strains (Eq I-6, Ibid.), and by not distinguishing between composite and constituent strains. Thus, their assertion that cylinders of small thickness will have "very high radial stress" is misleading (see Eq 17 and 18, above).

Equation 15 shows that the maximum mechanical strain in the radial bundles exceeds the maximum hoop-bundle mechanical strain by a quantity that depends strongly on the anisotropy of composite thermal expansion. Whether the radial bundles will actually experience such high mechanical strains will depend on whether they remain bonded to the rest of the composite (as has been assumed in Eq 3), the nature of frictional load transfer between debonded radial bundles and the rest of the composite, and whether creep-relaxation processes are of significance. These matters are under continuing study in this program, and at U.C.L.A under George Sines.

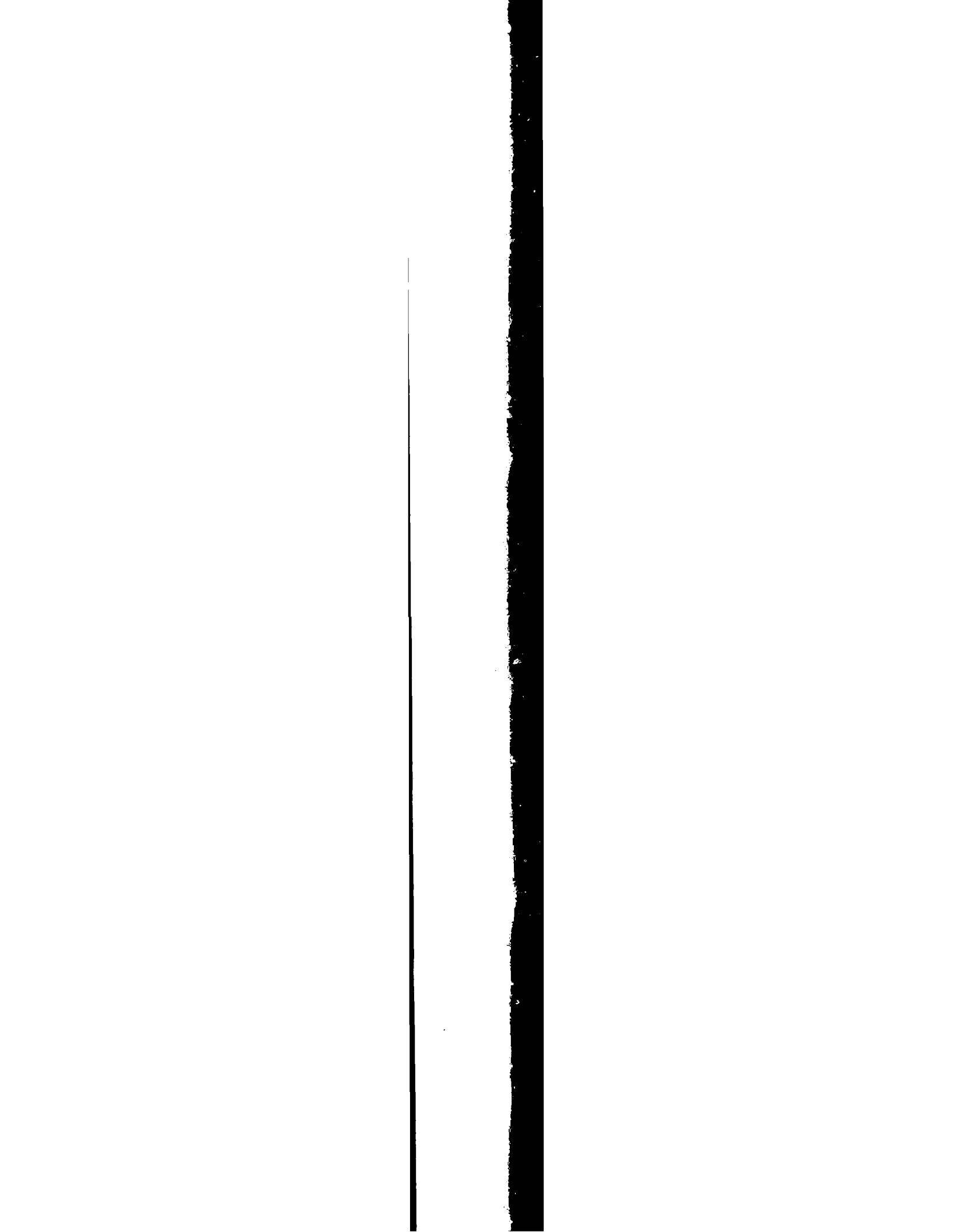
#### OCCURRENCE OF RADIAL-YARN FRACTURES

If the radial bundles do indeed experience stresses higher than do the circumferential (hoop) bundles, we would expect to see broken radial bundles in those billets that have fractured hoop bundles as a result of heat treatment. For billet designs that are marginal with respect to hoop-bundle fracture, we would expect to see some radial-bundle breaks without hoop-bundle fractures. Note, however, that radial-bundle breaks are not necessarily as obvious as hoop bundle breaks; because the composite's radial stress is compressive, radial bundles may be broken without resulting in macrocracking on planes normal to the radius. Hoop-bundle breaks, on the other hand, may propagate into macrocracks because of the composite's tensile hoop stress.

Radial-bundle breaks have been observed, with and without accompanying hoop-bundle fractures. During the 7-inch Program (Ref. 16), broken radials were seen in Billet A9, a pitch fiber billet that fractured across the hoop bundles during heat treatment (Ref. 17, 18, and 19). Billet A8, a sister billet to A9, was cut in half lengthwise after A9 failed; one half completed processing with an overwrap layer of circumferentially wound graphite yarn, the other completed processing without overwrap; neither half fractured in processing but both halves had broken radial yarns (Ref. 17). Billet F14, which survived processing without gross hoop fracture, also showed broken radials (Ref. 17).

Special attention was given to the radials in billets A8 and F14 because they were processed together with the fractured billet A9. Have other instances of broken radials occurred undetected, in process runs that have not resulted in catastrophic failures? Probably. For example, Billet G18 (a 7-inch Program billet) was found to have some broken radials (Ref. 20) only after a chance review of routine photomicrographs. Recently, on reviewing other microscope mounts of samples from the 7-inch Billet Program (supplied courtesy of F. I. Clayton of SAI), broken radials were found near the outer diameter of Billet F16.

To break the radial bundles, sufficient load transfer must occur (by shear) between the radial bundle and the surrounding composite near the free surfaces of the billet (the inner and outer radii). If the





When the composite fails, such load is promoted by the compressive stress along the axis, and by mechanical effects, and would be less efficient than an intact bond (see Appendix B). In continuous around the billet so hoop stress can be alleviated by interface shear. This can occur in the absence of radial stress. Bundles debond and slip within the

All yarns would be expected to reduce the elastic response of the composite. Thermal expansion in the radial direction causes radial yarns break or slip. In spite of the composite's radial Young's modulus, the decreased effectiveness of hoop stress in the outermost hoop bundle. Whether slippage or breakage can be explored analytically.

Relaxation processes are unlikely to occur below the hoop-bundle stresses; that also tend to reduce the hoop-bundle stresses. We have experienced hoop-bundle fractures, if any such billets exist, seem the likeliest explanation for the We should look carefully at all to establish the extent of radial-bundle of debonding. Noting whether the inner and outer diameter surfaces debonding; the amount of surface is estimated using a shear lag analysis

It would also be explained if the radial yarns. The theory of Appendix A suggests if they are subject to greater transverse Quantitative exploration of this hypothesis

Ch

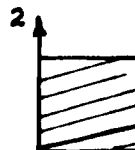
## EFFECTS OF STRAIN-INDUCED STRESS-STRAIN

The stress-strain behavior is affected significantly by strain-induced stresses in the constituents (eg, the fibers) to describe the stresses and strains.

Beyond Drucker's provocative work dealing with mechanisms of bimodal behavior, there appears to be little discussion concerning the effects of strain-induced stresses. Perhaps this lack of attention is due to the fact that the effects are of secondary importance in composites when the deformations are small. However, as shown below, that such effects are of primary importance, even for small deformations, in composites for which the ratio of fiber to matrix stiffness is unusually high. Thus, the material rotations are important in high-modulus graphite fibers in ceramic-matrix composites, as is usually the case with ceramic-matrix composites.

### ILLUSTRATIVE EXAMPLES

Consider a unidirectionally aligned fiber (in the direction) subjected to stresses



The stress-strain relation in the direction,  $\theta$ , between the fiber axis and the

$$\{\sigma\} = [C'] \{\epsilon\}$$

$$[C'] = fcn$$

\* I will appreciate being told of

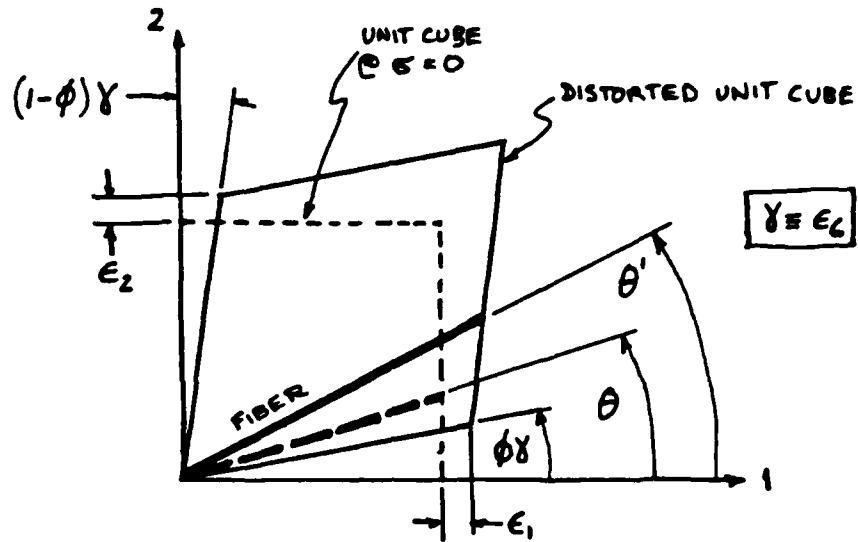


Figure 2. Effects of strain on texture angle.

Contracted notation is used for the strain subscripts, so, in terms of the Cartesian tensor components:  $\epsilon_1 = \epsilon_{11}$ ,  $\epsilon_2 = \epsilon_{22}$ ,  $\epsilon_6 = 2\epsilon_{12}$

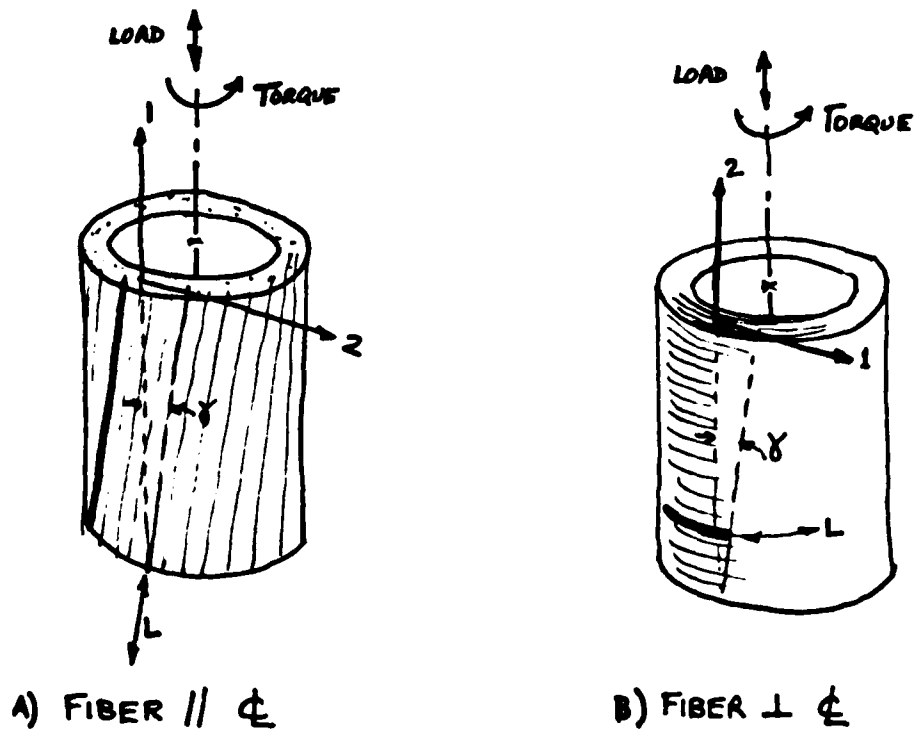


Figure 3. Illustrating the effect of a structure's geometry and loading conditions on the sensitivity of fiber orientation to shear strain.

where:

- $\sigma, d\sigma$  = stress, stress increment in 1,2 coordinates  
 $\epsilon, d\epsilon$  = strain, strain increment in 1,2 coordinates  
 $[C]$  = composite stiffness, in 1,2 coordinates  
 $[C]$  = composite stiffness, in L,T coordinates  
 (L = fiber direction, T is perpendicular to L)

The use of increments of stress and strain, in Eq 1, is necessary because  $\theta$  is a function of strain (Figure 2). At small strains, the strain-dependence of  $\theta$  is (after Ref. 1):

$$\theta' = \arctan \left[ \frac{(1 + \epsilon_2) \tan \theta + \phi \gamma}{1 + \epsilon_1 + (1 - \phi) \gamma \tan \theta} \right] \quad (3)$$

The proper value of  $\phi$  for analysis of a given structure depends on the loading situation and geometrical constraints. For example, in a test of a cylinder with axially-aligned fibers, subjected to torsion and axial load (Figure 3a), the entire shear strain is effective in rotating the fibers, so that  $\phi$  is effectively one if we maintain the 1,2 coordinates aligned with the applied loads. Alternatively, in a similar test of a transversely-aligned cylinder (Fig 3b) there is no rotation of fibers in the load-aligned 1,2 coordinates, so  $\phi$  is effectively zero. For uniform stress-states,  $\phi$  may in general take on any value between 0 and 1 (eg, Figure 4); and when a structure is subjected to gradients of stress, there may be additional rotations imposed by deformations outside the unit cell in question.

One implication of the strain-induced rotation of fibers, which has been discussed in Ref. 1, is the occurrence of bimodular behavior whenever the initial value of  $\theta$  is neither zero nor 90 degrees. Significant differences between tensile and compressive (secant-value)

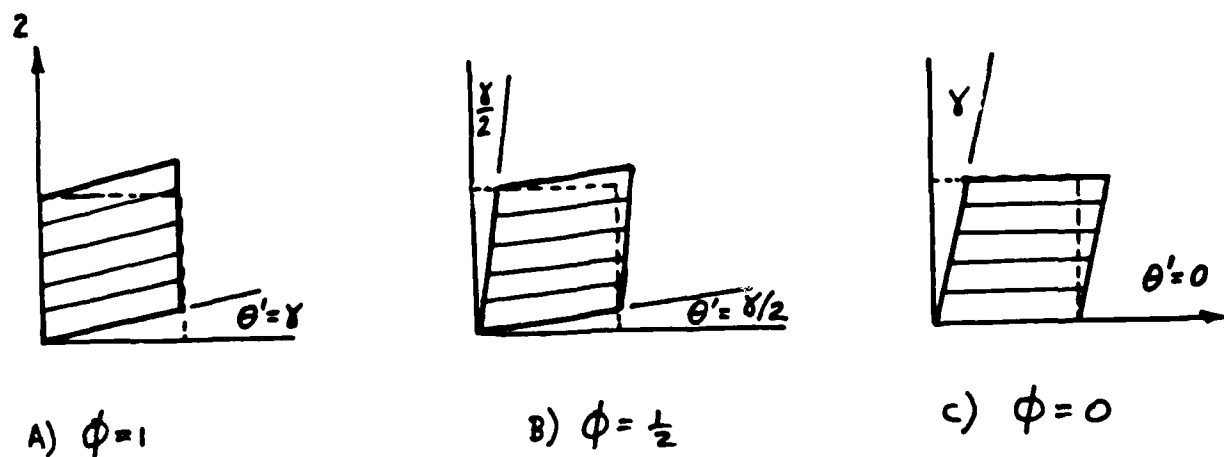


Figure 4. Illustrating the factor  $\phi$  and dependence of microscale rotation on coordinate definitions.

stiffnesses in the 1-direction are predicted for rather small initial values of  $\theta$  when the ratio of the extensional modulus of the composite,  $E_L$ , to its longitudinal shear modulus,  $G_{LT}$ , is high (in the order of 100, as is the case for high-modulus carbon-carbons); the difference between tensile and compressive responses depends on the applied stress magnitude, resulting in nonlinear tensile and compressive stress-strain responses.

Another consequence is that application of shear in combination with tension or compression can significantly affect the tensile or compressive response, even if the initial value of  $\theta$  is zero. For example, consider the simultaneous application of shear and compression to a unidirectional composite, as in the torsion test of Figure 3a; data from such a test would include plots of compressive stress vs compressive strain ( $\sigma_1$  vs  $\epsilon_1$ ) and shear stress vs shear strain ( $\sigma_6$  vs  $\epsilon_6$ ). Figure 5a shows the approximate effect of shear strain on the slope of the compressive stress-strain curve of a composite with a ratio of  $E_L$  to  $G_{LT}$  of 200, for various ratios of applied strain increments. It turns out (Fig. 5b) that the slope of the shear stress-strain curve is also affected by shear strain. Derivation of Figure 5 is described in the paragraphs below.\*

Upon introducing a shear strain, as in Figure 3a or Fig. 4a, the composite's fibers are no longer aligned with the direction of "axial" loading. For loadings in which  $\sigma_6$  (12-shear) is the only shear stress, Eq 1 may be expanded to give:

$$\begin{Bmatrix} d\sigma_1 \\ d\sigma_2 \\ d\sigma_3 \\ d\sigma_6 \end{Bmatrix} = \begin{bmatrix} C'_{11} & C'_{12} & C'_{13} & C'_{16} \\ C'_{12} & C'_{22} & C'_{23} & C'_{26} \\ C'_{13} & C'_{23} & C'_{33} & C'_{36} \\ C'_{16} & C'_{26} & C'_{36} & C'_{66} \end{bmatrix} \begin{Bmatrix} d\epsilon_1 \\ d\epsilon_2 \\ d\epsilon_3 \\ d\epsilon_6 \end{Bmatrix} \quad (4)$$

where the  $C'$  terms are the stiffnesses of the unidirectional composite tilted through the angle  $\gamma$  ( $= \epsilon_6$ ). By equating the tilt angle to  $\gamma$ , we are assuming that the current extensional strains are small enough to have negligible effect on fiber orientation (see Eq 3).

For illustrative purposes, we simplify by assuming  $d\epsilon_2$  and  $d\epsilon_3$  are negligible:

$$d\sigma_1 = C'_{11} d\epsilon_1 + C'_{16} d\epsilon_6 \quad (5)$$

$$d\sigma_6 = C'_{16} d\epsilon_1 + C'_{66} d\epsilon_6 \quad (6)$$

\* Analysis of this case was motivated by peculiarities of data from torsion-compression tests conducted on 3D carbon-carbon at Lockheed Missiles & Space Company (Ref. 22).

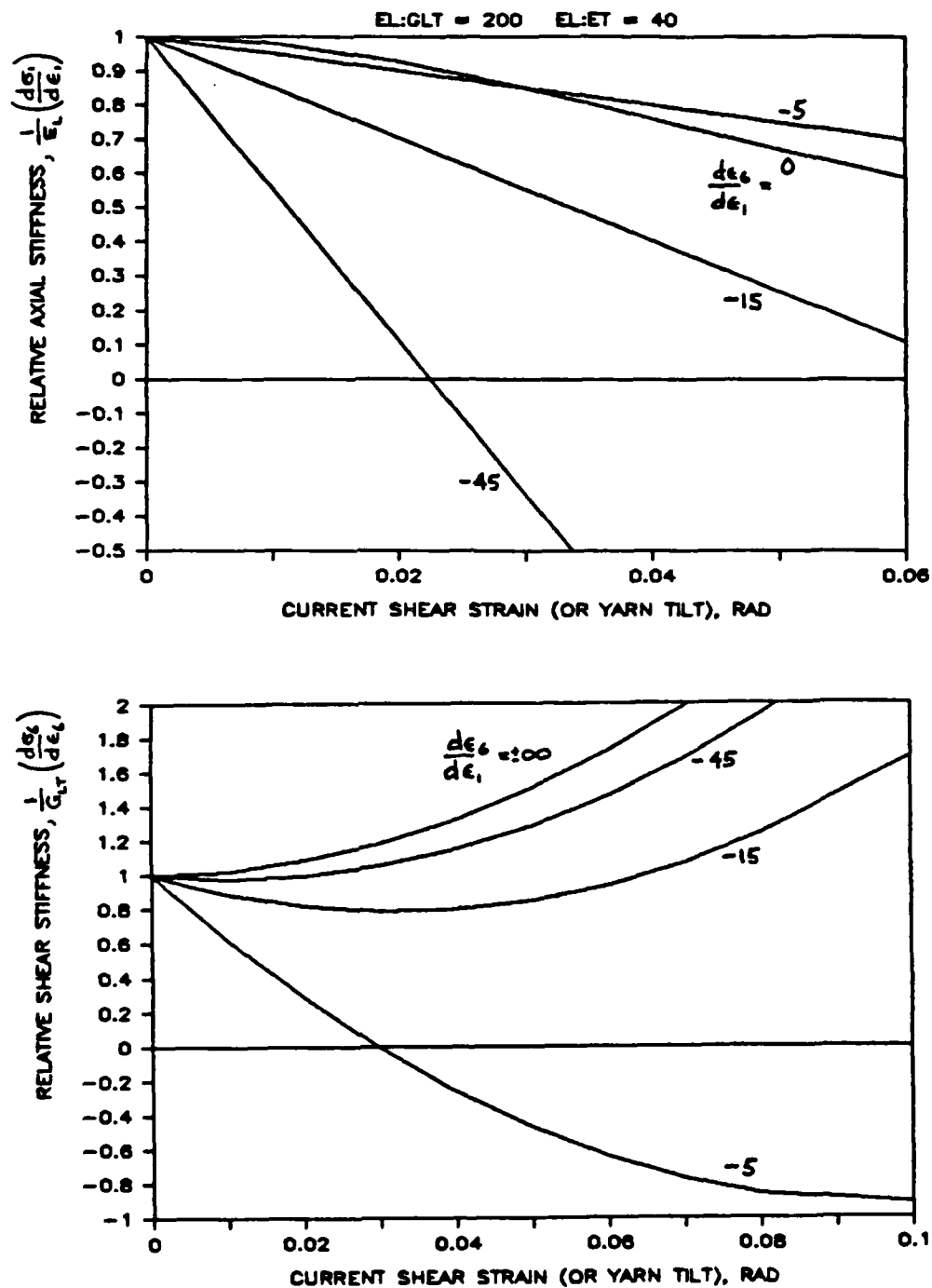


Figure 5. Effects of current shear strain, and ratio of applied shear strain increment to applied axial strain increment, on slopes of stress-strain responses in combined shear-compression loading. Top graph shows slope of compressive stress-strain curve. Lower graph shows slope of shear stress-strain curve.

The slopes of the extensional and shear stress-strain curves are then:

$$\frac{d\sigma_1}{d\epsilon_1} = C'_{11} + C'_{16} \frac{d\epsilon_6}{d\epsilon_1} \quad (7)$$

$$\frac{d\epsilon_6}{d\epsilon_6} = C'_{66} + C'_{16} \frac{d\epsilon_1}{d\epsilon_6} \quad (8)$$

To proceed, we express the  $C'$  in terms of the angle  $\gamma$  and the stiffnesses,  $C$ , of the composite in the L,T coordinate frame, by applying the appropriate rotational transformation (eg, Ref. 24):

$$C'_{11} = m^4 C_{11} + n^4 C_{22} + 4m^2 n^2 C_{66} \quad (9)$$

$$C'_{66} = m^2 n^2 C_{11} + m^2 n^2 C_{22} + (m^2 - n^2)^2 C_{66} \quad (10)$$

$$C'_{16} = m^3 n C_{11} - m n^3 C_{22} + 2(mn^3 - m^3 n) C_{66} \quad (11)$$

where  $m = \cos \gamma$  and  $n = \sin \gamma$ .

The numerical results shown in Figure 5 were obtained using the following input properties:

Longitudinal stiffness of 1D composite,  $C_{11} \cong E_L = 40$  Msi

Transverse stiffness of 1D composite,  $C_{22} \cong E_T = 1$  Msi

Shear stiffness of 1D composite,  $C_{66} = G_{LT} = 0.2$  Msi

which are more-or-less representative of the effective properties of the yarn bundles in graphitized 3D carbon-carbons made with high-modulus fiber. The assumed shear stiffness approximates the initial shear modulus for some 3D composites; because of the markedly nonlinear stress-strain response in shear, lower values, in the vicinity of .05 Msi, would apply at shear strains greater than about .005. Note also that, for the range of fiber tilt angles shown, the results are fairly insensitive to the value of  $E_T$ .

The trends shown in Figure 5 would be nearly unchanged if we considered a 3D composite instead of a 1D composite, assuming that the 3D is oriented to have one set of yarns axially aligned. This is because the axial stiffness of the 3D composite is controlled by the yarns in the axial direction.

The slopes of the stress-strain curves may be expressed also in terms of the ratio of applied stress increments, by inverting Eq 7 and 8 to get:

$$\frac{d\sigma_1}{d\epsilon_1} = \left[ S'_{11} + S'_{16} \frac{d\epsilon_6}{d\epsilon_1} \right]^{-1} \quad (12)$$

$$\frac{d\epsilon_6}{d\epsilon_6} = \left[ S'_{66} + S'_{16} \frac{d\sigma_1}{d\sigma_6} \right]^{-1} \quad (13)$$

where:

$$\begin{aligned} S'_{11} &= A C'_{66} \\ S'_{66} &= A C'_{11} \\ S'_{16} &= -A C'_{16} \\ A &\equiv [C'_{11} C'_{66} - (C'_{16})^2]^{-1} \end{aligned}$$

This may be a more convenient formulation for tests in which the load ratio rather than the strain ratio is controlled.

Of course, the sensitivity to shear implies a sensitivity to initial misalignments between the load axis and the fibers; for example, a misalignment of only one degree can have fairly large effects, as it corresponds in Figure 5 to a shear strain of about .017. Figure 6 presents much the same information as Figure 5, except in terms of the ratio of applied stress increments (Eq 12 and 13); also, Figure 6 shows the effect of negative tilt angles, as might occur with initial misalignment of the composite.

#### CONCLUDING REMARKS

The bimodularity described in Ref. 1 and the dependence of tangent stiffnesses on shear strains, shown in Figures 5 and 6, result from strain-induced changes in angle between the fibers and the applied stress. The sensitivity of stiffness to such changes in angle depends primarily on the ratio of  $E_L$  to  $G_{LT}$ . In Figure 7, we see that conventional advanced composites, such as graphite/epoxies (which have  $E_L : G_{LT}$  ratios in the order of 10\*), are much less sensitive to microscale rotations than are carbon-carbon composites, which may have stiffness ratios of several hundred. Also, while some 3D carbon-carbons can experience shear strains greater than .05 without failure, the strain levels at which Gr/Ep composites operate are usually less than .01. Thus, there appears to be little or no need to consider strain-induced fiber rotation for conventional epoxy-matrix composites. Nevertheless, it might be worthwhile to explore the issue further for conventional composites because there may be conditions (eg, high ratios of shear stress increment to axial stress increment) at which the effects of fiber rotation would be of technical significance.

Conventional small-strain constitutive relations, which do not account for strain-induced fiber rotations, would predict the stiffnesses corresponding to zero shear strain in Figures 5 and 6. Conventional stress-strain laws therefore could be seriously in error (sometimes by factors of more than two) for materials with large ratios of  $E_L$  to  $G_{LT}$ . The error depends on the stress or strain path in multiaxial loading.

\* The ratio of extensional to shear moduli for a T300/Epoxy composite ranges from about 2.5, for a quasi-isotropic crossply laminate, to about 25 for a unidirectional tape (Ref. 23).

While the preceding analysis has assumed a unidirectional composite, the results also illustrate the behavior of 3D composites; the stiffness of a 3D carbon-carbon, in a direction nominally parallel to one set of fibers, is determined primarily by the effective stiffness of those fiber bundles; thus, the relative stiffnesses plotted in Figures 5 and 6 are approximately applicable to 3D composites.

The need to account for strain-induced fiber rotations introduces the requirement that  $\phi$  (Eq 3) be defined. This complicates stress analysis, and suggests that some aspects of finite (large strain) elasticity theory be incorporated into the analysis of 3D carbon-carbon structures that experience multiaxial states of stress.

The results presented above are illustrative, take advantage of simplifying assumptions, and are intended primarily to justify the need for further work. Research appears necessary to address at least some of the following issues:

- a) What analytical approaches (eg, finite-element, or others) can provide adequate tracking of material orientations in a structural analysis? How can the required incremental analyses be accomplished efficiently and accurately?
- b) How can the actual initial orientations of fibers in a structure be identified (detected in practical environments and/or controlled in fabrication and assembly)?
- c) In the event initial orientations of fibers cannot be adequately controlled or known in practical situations, how should structural analyses deal with the resulting uncertainties in stress-strain responses?
- d) What experiments should be conducted to elucidate the multiaxial stress-strain behavior of such orientation-sensitive materials, and how is the data to be analyzed and used?
- e) How is the failure of orientation-sensitive materials affected by microscale material rotations? Should failure criteria be formulated in terms of actual orientations at failure? How?
- f) To what extent is the currently observed "variability" or scatter in property data the result of uncontrolled and unrecorded minor variations in initial material orientations?
- g) What are appropriate ways to formulate constitutive relations for orientation-sensitive materials? To what extent will it be necessary to include approaches used in large-strain or large-deformation theories?



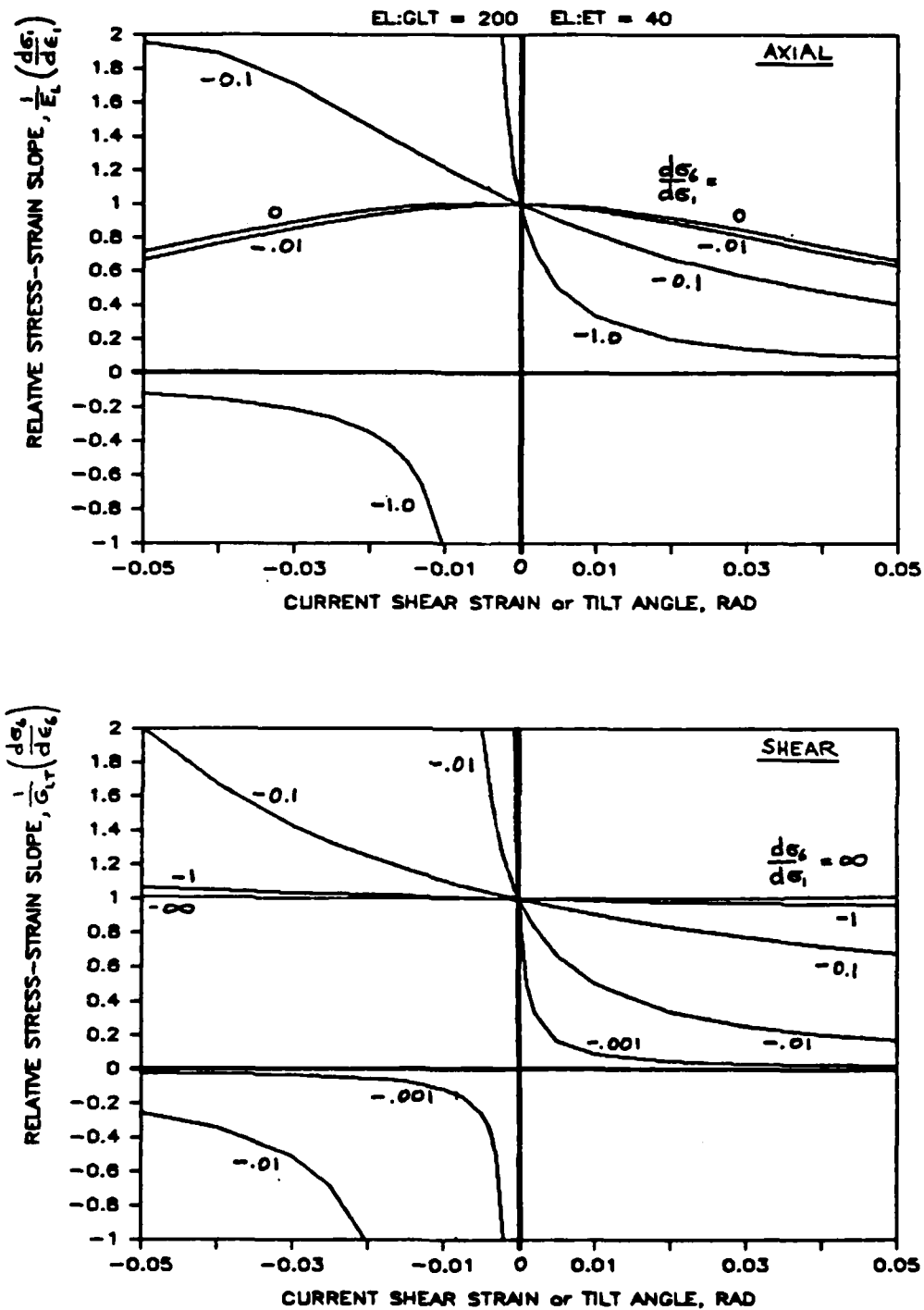


Figure 6. Effects of current fiber tilt angle, and ratio of applied shear stress increment to applied axial stress increment, on slopes of stress-strain responses in combined shear-compression loading. Top graph shows slope of compressive stress-strain curve. Lower graph shows slope of shear stress-strain curve.

h) For carbon-carbon composites, which are very orientation-sensitive and also exhibit nonlinear stress-strain behaviors, how are the effects of material orientation to be combined analytically with the effects of yielding, microcrack propagation, frictional behavior, etc.?

Our eventual goal should be the development of an approach, to structural design and analysis, of minimal complexity while nevertheless maintaining adequate accounting for the physical effects of strain-induced material rotations. It seems probable that good simple approaches will be possible only after detailed, and probably complex, studies of the issues listed above.

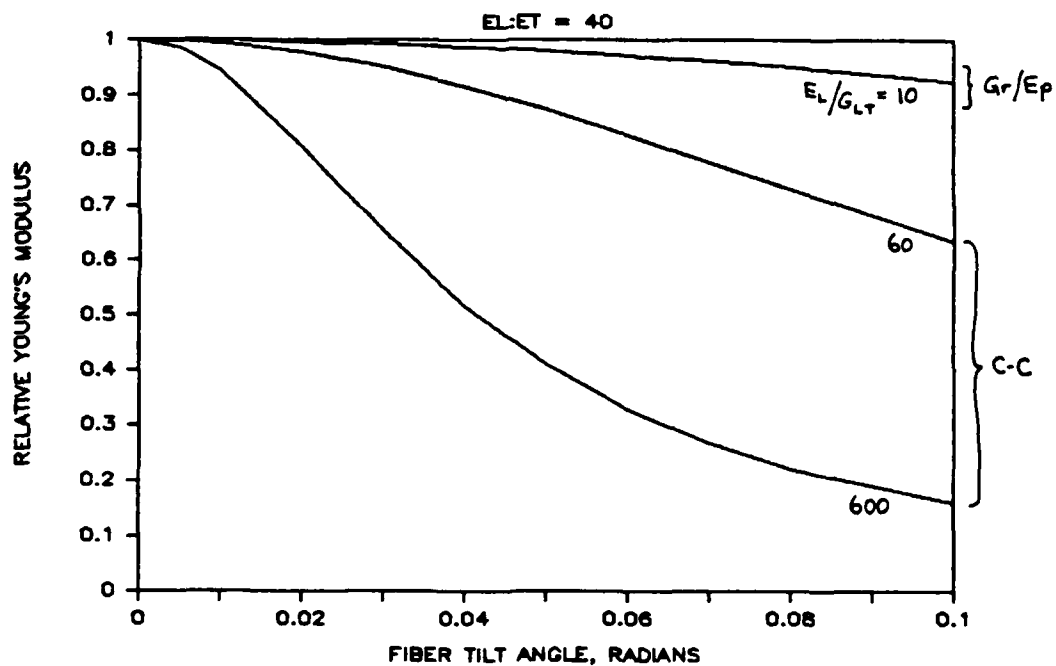


Figure 7. Effects of tilt angle on Young's modulus in uniaxial loading.

## APPENDIX A

**"A MODEL FOR TENSILE FRACTURE OF CARBON-CARBON COMPOSITE FIBER BUNDLES"**

The following pages are a copy of the paper presented to the JANNAF RNTS meeting in Huntsville, December 1984.



## A MODEL FOR TENSILE FRACTURE OF CARBON-CARBON COMPOSITE FIBER BUNDLES

Julius Jortner  
Jortner Research & Engineering, Inc.  
Costa Mesa, California

## ABSTRACT

A probabilistic model for tensile fracture of straight-fiber carbon-carbon composites is proposed. The analysis derives from the extensive theoretical work available for graphite/epoxy composites (eg, Batdorf, Manders et al, Rosen, and Phoenix), but attempts to account for the weak microcracked interfaces in carbon-carbons by assuming load transfer between fiber and matrix is primarily frictional. The model extends the work of Chatterjee, et al, by including a predictive analysis for the frictional shear stress, incorporating a Poisson's effect (from Gent) and a thermal-expansion effect. Inputs to the model include fiber, matrix, and interface properties (including friction coefficient), fiber strength distribution or the length dependence of dry-yarn strength, and transverse stresses acting on the yarn bundle. Illustrative results show that composite strength may be expected to increase with temperature even if the fiber strength does not. Also, the results show that room-temperature strength of a carbon-carbon yarn tends to be significantly lower than the strength of a similar graphite-epoxy yarn, even if no degradation of fiber properties has occurred during the fabrication of the carbon-carbon composite.

## INTRODUCTION

The effective strength of fibers in a carbon-carbon can be less than the average strength of the fibers. For a straight-fiber composite (eg, unidirectional, 2D tape laminate, or a Cartesian 3D block), the fiber utilization factor (or fiber strength efficiency) may be expressed as:

$$\eta = \frac{F_{ct}}{V_f \bar{\sigma}_f} \quad (a)$$

where  $F_{ct}$  is the composite tensile strength in the fiber direction,  $V_f$  is the fiber volume fraction in that direction, and  $\bar{\sigma}_f$  is the average fiber strength. Omission of matrix strength from Eq 1 appears reasonable for typical carbon-carbons ( $V_f = 10$  to 65 percent, approximately) because the matrix strength is much less than the fiber strength. Taking the values of  $\bar{\sigma}_f$  as they are reported by the fiber manufacturer, Table 1 provides some examples of fiber utilization factors for several carbon-carbon composites. These strength efficiencies are generally low, some being less than fifty percent. We might be tempted to ascribe the low efficiencies to "degradation" of the fibers during fabrication of the composite, or to misalignments of the fiber axis from the load axis (as in the undulations of yarns in a woven cloth composite). However, in judging whether or not fibers have been degraded or whether misalignment is a significant factor, it is necessary to estimate the strength of a similar straight-fiber composite in which no degradation has taken place.

Using a probabilistic approach, Chatterjee et al (Ref. 1) analyzed the on-axis tensile strength of fine-weave 3D carbon-carbons, made of T-50 (rayon) fibers, and concluded that the observed strength was approximately equal to the expected strength of a composite made with fibers having the strength variability observed in T-50 fibers and the weak interfaces typical of carbon-carbons. That is, the strength efficiency factor of about 60 percent (Table 1) for these composites can be explained in terms of the statistics of undegraded fibers. A similar conclusion would be reached for HM fibers in fine-weave 3D composites. However, the very low strength efficiency of carbon-carbons made with T-300 yarns (Table 1) probably cannot be attributed entirely to probabilistic effects. In such cases, the application of probabilistic theory would provide a baseline from which to estimate the extent of fiber degradation induced during fabrication of the composite.

We should note that the analysis of Chatterjee et al is incomplete in the sense that they backed into their conclusion by assuming no fiber degradation and finding that the consequences, in terms of certain initially unknown parameters (chiefly the strength of the fiber-matrix interface) used in their probabilistic model, appeared reasonable for carbon-carbons. In the probabilistic approach proposed here, an attempt is made to make analytical estimates of the fiber-matrix interfacial shear stress.

Prepared for presentation to the Sixth Rocket Nozzle Technology Meeting of the JANNAF PNTS, Huntsville, 6 December 1984.

Based on research sponsored by the Office of Naval Research under Contract N00014-82-C-0405.

Approved for public release; distribution is unlimited.

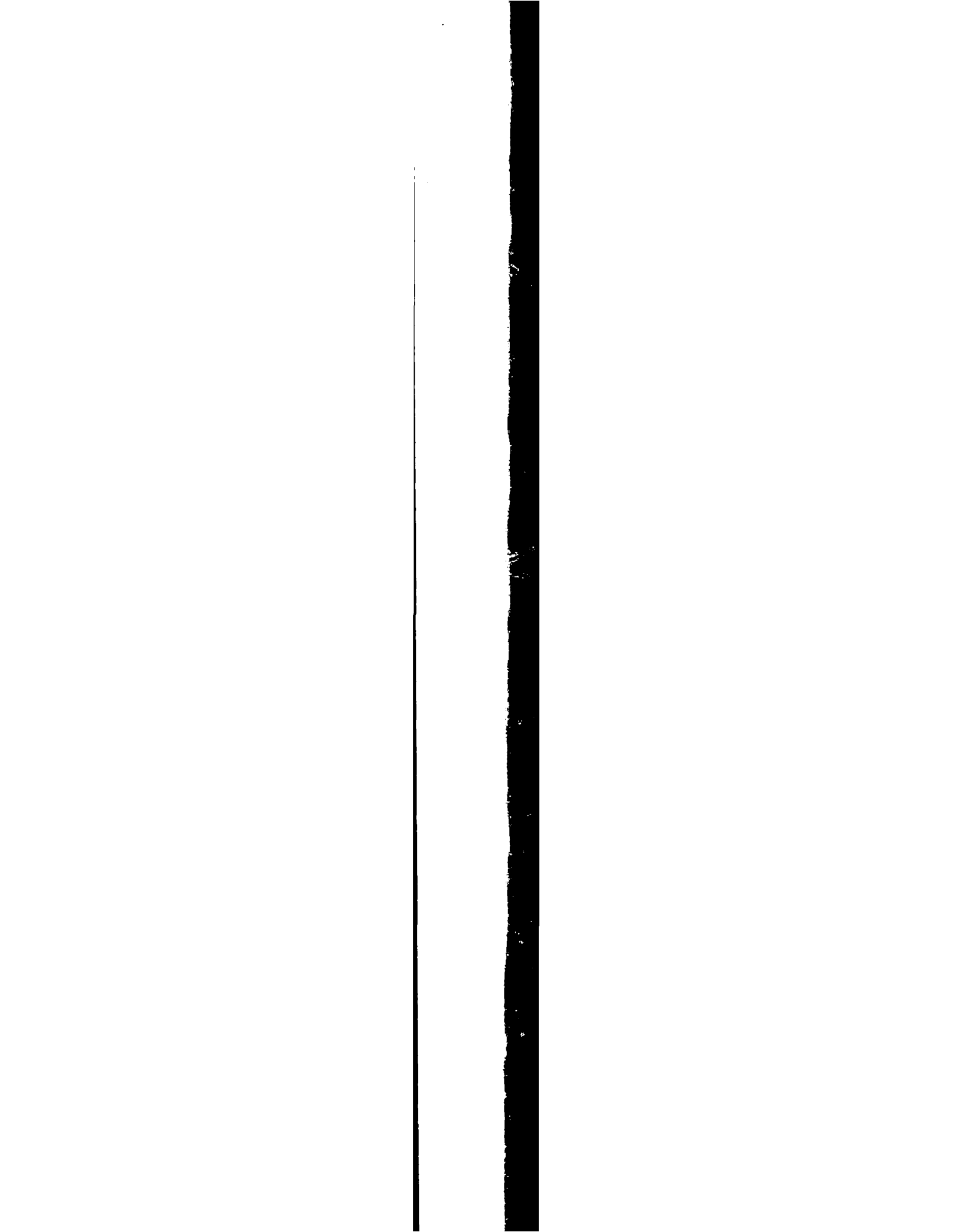


TABLE 1. STRENGTH EFFICIENCIES OF SOME CARBON-CARBON COMPOSITES @ ROOM TEMPERATURE

FIBER	AVERAGE FIBER STRENGTH KSI (approx.)	COMPOSITE TYPE	AVERAGE FIBER STRENGTH IN-SITU KSI (approx.)	STRENGTH EFFICIENCY FACTOR	SOURCE FOR COMPOSITE DATA (see notes)	REMARKS
T-50 (rayon)	315	3D block	190	0.60	A	fine-weave Cartesian
HM (PAN)	340	3D block	215	0.63	B	fine-weave Cartesian
T-300	400	3D cylinder	100	0.25	C	various woven cylinders
T-300 heat-treated	350	3D cylinder	100	0.29	C	same woven billets, treated T-300 assumed equivalent to T-50 PAN
T-300 heat-treated	350	2D laminate (8-harness satin cloth laminate)	160	0.46	D	ACC-4 w/o inhibitors, warp direction
WYB (rayon)	90	2D laminate (plain-weave cloth laminate)	21	0.23	E	KKARB 1200 involutes, warp direction
Japanese (PAN?)	286	unidirectional 50 % vol. fraction	110	0.38	F	experimental composite with furfural alcohol based matrix
Japanese (PAN?) treated to 2800 C	146	unidirectional 50 % vol. fraction	110	0.75	F	same composite as immed. above referred

Fiber strength data from compilations from Ref. G, Ref. H and Union Carbide literature.  
Japanese PAN data from Ref. F.

In-situ fiber strength estimated from on-axis composite strength using estimated fiber volume fraction.

Sources for data are:

- A. Littleton, H. E., and Pears, C. D., Mechanical, Thermal and Nondestructive Characterization of GE-2.2.3, AFML-TR-77-48, April 1977.
- B. Pears, C. D., et al, Evaluation of C-C Composites for the P4 Program, AFML-TR-78-2, Feb 1979.
- C. Kibler, J. J., In-Situ T-300 Fiber Properties in Tension and Compression in Carbon-Carbon Cylindrical Weaves, 1983 JANNAF RNTS Mtg, Colorado Springs, Dec. 1983.
- D. Starrett, Stuart, Prelim. Data for Structural Carbon-Carbon Composites, SoRI-EAS-84-9, Dec 1983.
- E. Davis, H. O., and Vronay, D. F., Structural Assessment of Involutes, AFML-TR-79-4068, June 1979.
- F. Yamada, Shigehiko, and Tamada, Koshi, Graphitization of Carbon-Fibre/Glassy Carbon Composites, J. Comp. Mat., reprinted in Carbon Composite and Metal Composite Systems, C. J. Hilado, Ed, Technomic Publishing Co, 1974, pp18-21.
- G. Schmidt, D. L., Replacement Fibers for Thermal Protection Applications, AFML-TR-77-68, Aug 1977.
- H. Chard, W. and McCall, J., Assessment of the Availability and Utilization of Carbon-Base Fibers for DoD Applications, Part I - Final Report Summary, Battelle Columbus Labs, December, 1977.

characteristics of the fiber-matrix interface. Because of the stress concentrations surrounding a fiber break, the composite strength is lower than would be predicted by the Rosen model for the same effective length. For the composites considered by Manders et al, the difference between the strengths predicted by the coupled-bundle model and the Rosen model is small (about five percent, Ref. 2).

Applying the coupled bundle analysis to new composites requires estimates of the effective length and the stress-concentrations. For graphite/epoxy composites, in which the matrix and interface bond are reasonably effective, the effective length has been estimated to be in the vicinity of 10 fiber diameters, and the peak stress in near-neighbor fibers is estimated to be about 25 percent higher than the average fiber stress (Ref. 2). The effective length increases if the matrix debonds locally from the broken fiber; the debond length is undoubtedly a function of applied stress, and the stress concentration is probably lower for longer debonds. Given the weakness of graphite matrices in shear, and the ubiquitous microcracking observed in composites that have been processed at high temperatures, it is likely that the effective lengths for carbon-carbon composites are very much longer than for epoxy-matrix composites. Chatterjee et al (Ref. 1) have estimated the effective length in 3D carbon-carbons to be of the order of 1 inch, which translates to more than a thousand fiber diameters; they treat the load transfer in a carbon-carbon as being frictional (across a debonded interface) and the effective length  $\delta$  as being proportional to the inverse of the frictional shear stress  $\tau$  :

$$\delta = \frac{\bar{\sigma} r_f}{\tau} \cong \frac{\sigma_c r_f}{\tau v_f} \quad (4)$$

where  $\bar{\sigma}$  is the average fiber stress,  $\sigma_c$  is the stress applied to the 1D composite,  $v_f$  is the fiber volume fraction, and  $r_f$  the fiber radius. The shear lag distance over which elastic stress transfer occurs can be shown small in relation to Eq 6, if  $\tau$  is small relative to the interface shear strength and the fiber stress is high (Ref. 1).

Given the small difference between coupled bundle predictions of composite strength and the predictions of the Rosen model (Manders et al, Ref. 2), and the decrease in coupling (stress concentration) that occurs as effective length increases, it is probably adequate to avoid the complications of coupled-bundle theory and use the uncoupled Rosen approach in treating carbon-carbons. Thus, being ignorant of the actual stress concentration factor is relatively unimportant, and the chief unknown becomes the frictional shear stress (Eq 6). This is the basis for Chatterjee et al's analysis (Ref. 1), shown schematically in Figure 1.

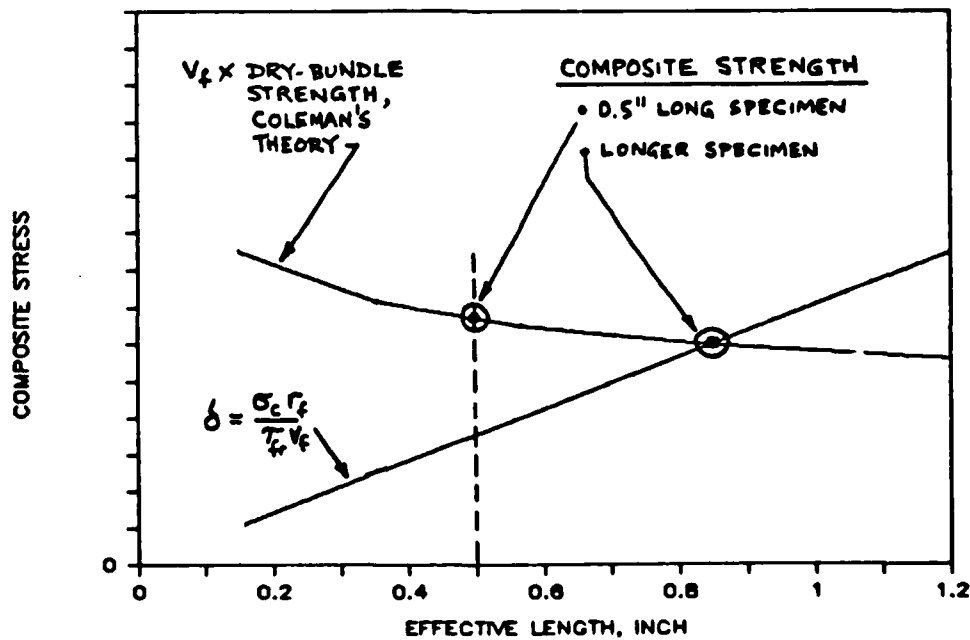


Figure 1. Schematic of the tensile fracture model of Chatterjee et al (Ref. 1).



The graph of Figure 1 is based on the use of Equation 6 to predict effective lengths that are linear with applied stress, assuming a constant value for the frictional shear stress. Fracture of the composite is predicted at an applied stress large enough that the effective length becomes such that the uncoupled-bundle strength is equal to the average fiber stress. An approximate limit to the effective length is the gage length  $L_G$  of the composite tensile specimen; if this limit is reached first, the composite strength estimate is the dry-bundle strength for bundles of length  $L_G$ .

If the fiber strength distribution is known and complies well with the Weibull equation (Eq. 3), the composite bundle strength curve in Figure 1 can readily be constructed from the Coleman analysis (Eq 5), the weakest link scaling law (Eq 1), using the volume fraction of fibers as the factor relating dry bundle strength to composite bundle strength. Alternatively, the composite bundle strength curve can be obtained from directly measured strengths of dry bundles of various lengths (as was done in Ref. 1); again, the composite bundle strength is the dry bundle strength multiplied by the fiber volume fraction.

#### NEW ANALYSIS

We proceed to extend the approach illustrated in Figure 1 by estimating the frictional shear stress as a function of the properties of the fiber, matrix, and their interface.

Assuming simple friction, the shear stress would be the product of the compressive radial stress across the interface and the friction coefficient. The radial stress could arise from two effects: a temperature-dependent compressive stress arising from the thermal-expansion mismatch between the fiber and the surrounding composite, plus a compressive stress that results from the Poisson's expansion of the fiber radius when the axial fiber stress is released; the concept of the Poisson's effect is suggested by the work of Gent (Ref. 4), for example.

The analysis proceeds by considering a (virtual) gap at the fiber-matrix interface (schematically shown in Fig. 2). On loading the composite in tension to stress  $\sigma_c$  the outer radius of the gap shrinks by Poisson's effect:

$$\Delta r_m = -\nu r_m \frac{\sigma_c}{E_{cL}} \quad (7)$$

where  $E_{cL}$  is the axial Young's modulus, and  $\nu$  the axial Poisson's ratio, of the uni-directional composite. Under loading, the fiber radius also shrinks. However, when the fiber breaks its radius springs back to the original unloaded value,  $r_f$ . The change in gap, at the broken end of the fiber, is then:

$$\frac{\Delta g_p}{r_f} \equiv \frac{\Delta r_m}{r_m} = -\nu \frac{\sigma_c}{E_{cL}} \quad (8)$$

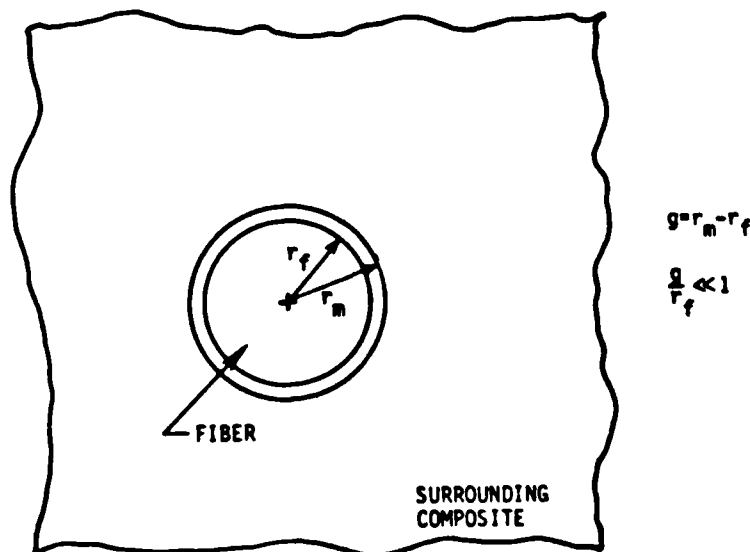


Figure 2. Idealization of fiber-matrix interface.

assuming that the gap  $g$  is small in relation to the fiber radius. The gap is also affected by heating the composite, as a result of the difference between transverse expansivity of the fiber  $\alpha_{fT}$  and that of the composite  $\alpha_{cT}$ :

$$\frac{\Delta g_T}{r_f} \cong (\alpha_{cT} - \alpha_{fT}) \Delta T \quad (9)$$

where  $\Delta T$  is the temperature rise. The net change in gap, at the broken end of the fiber, is:

$$\Delta g = \Delta g_P + \Delta g_T \quad (10)$$

To account simply for the gradient in fiber tensile stress as frictional shear introduces load near the broken end, we use an estimate of the average gap change  $\bar{\Delta g}$ :

$$\bar{\Delta g} \cong \frac{1}{2} \Delta g_P + \Delta g_T \quad (11)$$

This simple averaging assumes that the Poisson's ratio of the fiber is approximately equal to that of the composite bundle. The effect of this average gap change on radial stress across the fiber-matrix interface may be estimated (by analogy to a cylindrical shrink fit, Ref. 7, for example) to be, approximately:

$$\bar{\sigma}_R \cong \frac{\bar{E}_T \bar{\Delta g}}{2 r_f} \cong \frac{\bar{E}_T}{2} \left[ (\alpha_{cT} - \alpha_{fT}) \Delta T - \frac{\nu \sigma_c}{2 E_{cL}} \right] \quad (12)$$

where  $\bar{E}_T$  is an appropriate average of the composite's and the fiber's Young's moduli transverse to the fibers.

The total effective radial stress we use is the sum of  $\bar{\sigma}_R$  from Eq 12 and an initial radial stress  $\sigma'_R$ . The initial radial stress may be estimated as the sum of any residual transverse stress (arising from cooldown from the last process heat-treatment) plus any external tractions imposed on the yarn bundle (from stresses applied to the composite or from mini-mechanical interactions within a multi-directional composite). Thus, the frictional shear stress capability is:

$$\tau = -\mu (\bar{\sigma}_R + \sigma'_R) + \tau' \quad (13)$$

where  $\mu$  is the coefficient of friction and  $\tau'$  is a minimum frictional resistance due to other factors such as mechanical interlocking of micro-roughened interface surfaces.

The friction coefficient might be estimated from the extensive data available for graphites under friction (eg, Ref. 8 and 9). Unfortunately, the friction coefficient is affected significantly by various factors that are difficult to quantify for the composite, including adsorbed gases and the crystallographic nature of the surfaces. Thus, in the absence of direct data, we must guess the friction coefficients to implement this analysis.

The new analysis is the same as that of Chatterjee et al (Ref. 1) except that the shear stress used in Eq 6 is given by Eq 13, rather than taken as an arbitrary constant.

#### DISCUSSION OF LIMITATIONS

As noted in the development, the analysis is quite simplified. This is appropriate now because the experimental data (eg, Poisson's ratios of the fiber) necessary to support a refined analysis is not available. Also, by restricting the analysis to frictional shear lag, we have ignored the elastic shear lag. For the long effective lengths expected at low temperatures, this may be an appropriate approach. However, for some cases, it may be important to extend the model to include the elastic shear lag also.

If the fiber strength distribution cannot be well fitted by the Weibull distribution, two alternatives may be considered. Neither seems difficult to implement. The first approach would be to determine whether the low-probability-of-fracture "tail" of the strength distribution may be well fitted by a Weibull curve. If so, the analysis would proceed using the local distribution, with some obvious modifications to the Coleman equations. The rationale for doing so derives from the fact that a minor fraction of fibers in a bundle need to break before the bundle breaks (Ref. 2); thus, only the low-probability tail of a distribution and the average fiber strength need be known with any accuracy to predict bundle failure. If the tail of the distribution does not conform well to a Weibull curve, it would be desirable to use the fiber strength distribution, directly as

measured, by applying the chain-rule to shift it to the effective length, and by repeating Coleman's analysis numerically using the experimental distribution to predict bundle failure. Or, as pointed out earlier, data from strength tests on dry bundles of various lengths may be used directly.

The modeling described above assumes that the fiber bundle and a weak quasi-isotropic matrix are the constituents of the uni-directional carbon-carbon composite. This simplification ignores the possibility that a highly oriented matrix "sheath", which has been observed by microscope in several carbon-carbons (eg, Ref. 10 and 11), contributes to the composite strength. The role of the sheath is not well understood at present. Evangelides, Ref. 11 and 12, attributes to the sheath the observed fact that the effective Young's modulus of T-50 fibers in-situ is significantly greater than the virgin fiber modulus. Similar increases in effective fiber stiffness occur in composites made with other graphite fibers (eg, Ref. 13). However, factors other than the sheath may also contribute to the in-situ stiffening of graphite fibers; these include the fact that in-situ fiber density is higher than virgin fiber density, that the fibers undergo some stretching during the fabrication of carbon-carbons (Ref. 14 and 15), and that fiber properties are affected by temperature cycling (eg, Ref. 16); reasonable estimates of these effects can account for the magnitude of the stiffening (Ref. 14) without invoking the sheath effect.

Thus, it is not clear that the sheath actually plays the important role ascribed to it by Evangelides. The fact that the in-situ stiffness of pitch-densified 3D composites made with T-50 and T-75 fibers is the same (Ref. 13), in spite of a large difference in virgin-fiber stiffnesses, suggests that the sheath does not contribute significantly to the composite stiffness. At first glance, this conclusion may seem contradicted by the observed sheath-like orientations of matrices within c-c fiber bundles. However, when we consider the concurrent observation that the in-situ matrix is extensively microcracked, it does seem reasonable to discount its contribution to composite stiffness and strength, as in the simplified strength model described above.

As the uni-directional strength model depends heavily on good estimates of the interfacial friction, review of any available and relevant data is needed; also, new tests are recommended. Available data for quantifying the interfacial shear include experiments conducted in "microshear punch tests" on uni-directional composites (Seibold et al, Ref. 17) and on 3D and 4D composites (Loomis et al, Ref. 18). The test and representative load-deflection data are schematized in Fig. 3. In Seibold et al's tests, the punched-out plug is simply a portion of the uni-directional composite pushed out in the axial direction by the punch. In Loomis et al's tests, the punched-out plug is a complete yarn bundle pushed out of the surrounding 3D or 4D composite. While neither test directly deals with the fiber-matrix interface, the data is indicative of the general magnitude of the interface strengths in such composites. In the absence of a fiber pull-out or punch-out test, which would be difficult to perform because of the small dimensions of fibers, this seems as close as we can reasonably approach the required properties by experimentation.

The load-deflection traces in both Ref. 17 and Ref. 18 show a post-ultimate load that may be attributed to friction. Unfortunately, the friction observed in these tests includes friction between the punch and the composite, and the friction attributable to the plug-composite interface cannot be unambiguously derived from these tests. Indeed, the implied values of frictional shear stress are several hundred psi at room temperature, which (see Table 2) would imply rather (unreasonably?) short effective lengths in the composite.

To provide better friction data, a modified microshear test procedure has been suggested (Ref. 19). To avoid the punch-composite friction, the tests should involve changing to a slightly smaller diameter punch just after peak load is reached. In this way, the friction force will be due solely

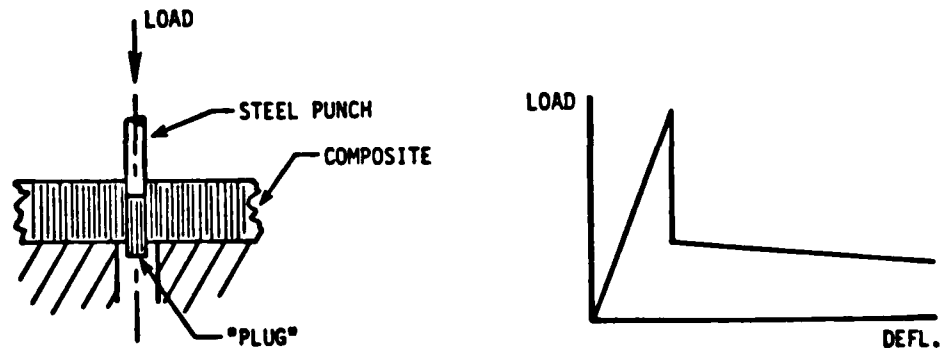


Figure 3. Schematic of the microshear punch test.

to plug-composite effects. An alternate approach would be to evaluate data from yarn pullout tests (such as are planned at UCLA, Ref. 22, or such as those described in Ref. 23). The analysis of punch-out data should account for the transverse compressive stress, generated by Poisson's expansion of the plug resulting from the axial punch force. An inverse Poisson's effect would occur in pull-out tests. The Poisson's effect may be treated in essentially the same manner as described above for the fiber-matrix friction, with consideration for the large difference between the Poisson's ratios of 3D composites and their yarns.

Experimental verification of the analytical model for tensile strength would include obtaining data regarding the effective length of the fibers within a composite. In the absence of direct data, effective length information most commonly is indirectly derived by comparing the behavior of the composite to the behavior of the fibers with the aid of a theory (eg, Ref. 3 or 4). There is, however, a more direct technique for dealing experimentally with the determination of effective length, described by Drzal (eg, Ref. 20). The method consists of testing a composite comprising one fiber in a relatively large volume of matrix, in axial tension, and observing under a polarizing microscope the occurrence and spacing of fiber breaks. This special uni-fiber composite is strained until no further fiber breaks occur; then the spacing between fiber breaks is readily interpreted to give estimates of effective length and interfacial shear strength. Currently, the method relies on transparency of the matrix for optical observations of fiber breaks, etc.. Application to opaque composites such as carbon-carbon would require additional development. At least two possible approaches might be attempted: destructive inspection of the specimens after test to measure the length of fiber fragments, or measurement (via Moire techniques or laser interferometry) and interpretation of surface strains to establish the spacing of fiber breaks during the test. Insofar as the Air Force Wright Aeronautical Laboratories currently is pursuing the application of the method to carbon-carbons (Ref. 21), we may anticipate interesting results.

The analysis presented here is relevant to multi-directional composites made with straight yarns. However, in a laminate or a 3D composite, failure of a bundle may not propagate to fail the composite, much as our tensile model shows that a single fiber break does not constitute failure of the bundle. Therefore, additional development of the tensile model may be necessary to deal with tensile fracture of multi-directional composites.

#### ILLUSTRATIVE RESULTS

For illustrative purposes, calculations have been done assuming  $\sigma_k$  and  $\tau'$  to be zero, and assuming the fiber strength distribution and the various thermal and elastic properties are independent of temperature. Table 2 shows the inputs and outputs of the analysis. Figure 4 is a plot of the results, in the same format as Figure 1. The results show that friction stress is dependent on yarn stress and temperature, and that the composite strength increases with temperature as is the case for real carbon-carbons (eg, Ref. 1).

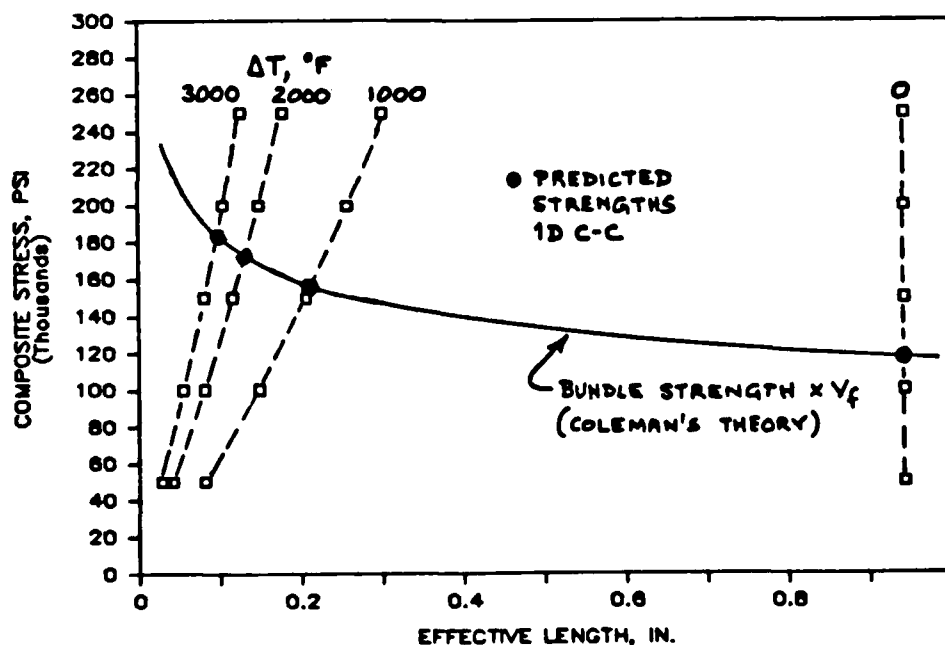


Figure 4. Illustrative results (see Table 2).

## CONCLUSIONS

The model for tensile strength, presented here, estimates the expected strength of a uni-directional carbon-carbon as a function of the strength distribution of the fibers, the gage length of the composite test specimen, the residual thermal stresses at the fiber-matrix interface, the expected friction coefficient at the fiber-matrix interface, the transverse thermal expansion coefficients of the fiber and matrix, the stresses applied to the composite, and the Poisson's ratio of the yarn bundle.. Discrepancies between measured composite strength and the analytical predictions can, if these input properties are sufficiently well known, be attributed to fabrication-process induced changes in the strength distribution of the fibers.

By including transverse compression stress as a parameter, the model suggests that the tensile strength of yarn bundles in a multi-directional composite will be affected by mini-mechanical stresses and by transverse tractions applied to the composite.

By including the properties of the matrix (insofar as it affects the transverse properties of the uni-directional yarn bundle), and the frictional behavior of the fiber-matrix interface, the model may find use in guiding the selection of matrices and processes for improving tensile strength of carbon-carbon composites.

TABLE 2. ILLUSTRATIVE CALCULATIONS FOR UNIDIRECTIONAL C-C.

INPUTS (HYPOTHETICAL COMPOSITE, INDEPENDENT OF TEMPERATURE):

Weibull Modulus, m	5	for 1" long
Weibull Scale Fact., sigO	300000 PSI	fibers
Composite Axial Modulus, E <sub>cL</sub>	4.00E+07	PSI
Avg Transverse Modulus, E <sub>barT</sub>	4.00E+05	PSI
Composite Poisson's Ratio, NU <sub>cLT</sub>	0.3	
Composite Expansivity, ALP <sub>cT</sub>	8.00E-06	per deg F
Fiber Expansivity, ALP <sub>fT</sub>	1.00E-05	per deg F
Fiber Volume Fraction, V <sub>f</sub>	0.65	
Friction Coefficient, MU	0.3	
Fiber Radius, R <sub>f</sub>	0.000138	inch

OUTPUTS:

TEMP. RISE	ASSUMED COMPOSITE STRESS	PREDICTED MAXIMUM FRICTION STRESS	PREDICTED EFFECTIVE LENGTH	THEORETICAL BUNDLE STRENGTH
deg. F	PSI	PSI	IN.	PSI
0	50000	11	0.9429	117081
0	100000	23	0.9429	117081
0	150000	34	0.9429	117081
0	200000	45	0.9429	117081
0	250000	56	0.9429	117081
1000	50000	131	0.0808	191372
1000	100000	143	0.1489	169361
1000	150000	154	0.2070	158561
1000	200000	165	0.2572	151825
1000	250000	176	0.3009	147126
2000	50000	251	0.0422	217911
2000	100000	263	0.0808	191372
2000	150000	274	0.1162	177953
2000	200000	285	0.1489	169361
2000	250000	296	0.1790	163228
3000	50000	371	0.0286	235608
3000	100000	383	0.0555	206337
3000	150000	394	0.0808	191372
3000	200000	405	0.1048	181692
3000	250000	416	0.1274	174717

The illustrative calculations have shown that increased strength at high temperatures may be expected for carbon-carbons, even if the fiber strength does not increase with temperature.

Given the expectation of weak fiber-matrix interfaces in carbon-carbons, the model suggests that carbon-carbon yarn bundles will be weaker than graphite-epoxy yarn bundles made with the same fiber, even if there is no degradation of fiber properties during making of the carbon-carbon composite.

Implementing the analysis requires much data that is currently unavailable or only poorly known. In particular, effort should be directed toward measuring transverse properties of fibers and interface strengths and frictional behavior. It is recommended that appropriate experiments be devised and conducted.

#### ACKNOWLEDGMENTS

Funding of this research by the Office of Naval Research and the encouragement and support offered by Dr. L. H. Peebles, Jr., ONR's Scientific Officer, are gratefully acknowledged. It also gives the author pleasure to thank, and acknowledge his considerable debt to, Dr. S. B. Batdorf for an informal education in the theories of composite tensile strength. Thanks are also due Mr. F. I. Clayton for helpful discussions and for introducing the author to the important paper by Manders, Bader and Chou.

#### REFERENCES

1. Chatterjee, S. N., McLaughlin, P. V., and Lowe, D. L., An Investigation of the Tensile and Shear Strengths of 3D Carbon-Carbon Composites, AIAA/ASME SDM Conference, 1976.
2. Manders, Peter W., Bader, Michael G., and Chou, Tsu-Wei, Monte Carlo Simulation of the Strength of Composite Fibre Bundles, Fibre Science and Technology, Vol.17, 1982, pp183-204.
3. Rosen, B. W., Tensile Failure of Fibrous Composites, AIAA J., Vol. 12, 1964, p1965ff.
4. Batdorf, S. B., A New Micromechanical Theory for Composite Failure, 1980 JANNAF RNTS Meeting, Monterey.
5. Phoenix, S. L., Probabilistic Strength Analysis of Fibre Bundle Structures, Fib. Sci. Tech., 1974, vol.7, p15ff.
6. Gent, A. N., Fracture Mechanics Applied to Elastomeric Composites, Rubber Chemistry and Technology, Vol.56, No.5, Nov-Dec 1983, pp1011-1018.
7. Den Hartog, J. P., Strength of Materials, Dover Press, 1949.
8. Reynolds, W. N., Physical Properties of Graphite, Elsevier, 1968.
9. Diefendorf, R. J., Proc. Conf. Carbon, 1959, p483ff and p489ff.
10. Jortner, J., Cracking in 3-D Carbon-Carbon Composites During Processing and Effects on Performance, Proc. Army Symp. Solid Mechanics, 1976, AMMRC MS 76-2, September 1976, pp81-97.
11. Evangelides, J. S., A Physically Based Analytical Tensile Model for Carbon-Carbon Composites, 13th Biennial Conf. Carbon, 1977, p351ff.
12. Evangelides, J. S., Microstructural Characterization of Crack Propagation and Analytical Modeling of Carbon-Carbon Composites, Proc. Army Symp. Solid Mech., AMMRC MS 76-2, Sept 1976.
13. Jortner, J., and Clayton, F. I., Carbon-Carbon Microstructure: Causes and Effects on Nosedip Ablation, McDonnell Douglas Report MDC G6390, April 1976.
14. Eitman, D. A., et al, Fiber Matrix Interactions in Carbon-Carbon Composites, 19th National Symposium SAMPE, April 1974.
15. Jortner, J., et al, In-Situ Densities of Fibers and Matrices in Carbon-Carbon Composites, McDonnell Douglas Report MDC-G7385, May 1978.

16. Albugues, F., et al, influence of High Temperature Thermal Treatments on the Properties of Carbon Fibers, Extended Abstracts of 16th Biennial Conference on Carbon, American Carbon Society, July 1983, pp492-493.
17. Seibold, R. W., et al, Advanced Densification of Carbon-Carbon Composites..., AFML-TR-79-4003, Feb. 1979.
18. Loomis, W. C., et al, Rocket Nozzle Processing Science (APIC/RN), AFWAL-TR-81-4118, November 1981.
19. Clayton, Fred I., Personal Communication, May 1984.
20. Drzal, Lawrence T., et al, Adhesion of Graphite Fibers to Epoxy Matrices, I. The Role of Fiber Surface Treatment, J. Adhesion, 1982, Vol. 16, pp1-30.
21. Drzal, L. T., Personal Communication, April 1984.
22. Sines, George, Personal Communications, 1984.
23. Jortner, J., Effects of Anomalies on Thermostructural Behavior of 3D Carbon-Carbon Composites, AFWAL-TR-82-4118, October 1982.

## APPENDIX B

**"EFFECTS OF SHEAR LAG ON THERMAL EXPANSION OF 3D CARBON-CARBON COMPOSITES"**

The following pages are a copy of the paper presented to the JANNAF RNTS meeting in Huntsville, December 1984.

PREVIOUS PAGE  
IS BLANK



## EFFECTS OF SHEAR LAG ON THERMAL EXPANSION OF 3D CARBON-CARBON COMPOSITES

Julius Jortner  
Jortner Research & Engineering, Inc.  
Costa Mesa, California

## ABSTRACT

The thermal expansion of coupons of 3D carbon-carbon is analyzed in terms of the thermo-elastic properties of the mini-constituents (yarn bundles and matrix pockets) and the stress transfer across their interfaces. The weakness of the interfaces limits the stress transfer by shear. When the shear strength of the interface is exceeded and debonding occurs, stress transfer in the de-bonded region is assumed to be frictional. The frictional shear capability is estimated as a function of the inter-constituent stresses that occur on heating. The analysis, which deals with the stress-transfer using a shear-lag approach, provides estimates of the displacements between mini-constituents. Numerical results are presented to show how elastic and frictional shear lag influences measurements of thermal expansion. The relation of specimen dimensions to the geometry of the composite's unit cell, and details of the measurement technique, are predicted to influence the measured expansions; for some techniques, the measured expansion is predicted to differ significantly from the true expansion of the bulk composite material. Analytical predictions are shown to compare reasonably well to Lander's data on end effects, up to about 4000 F, beyond which the likelihood of creep/relaxation phenomena makes the analysis inapplicable. Directions for improving the analysis are described, and requirements for experimental determination of input properties are identified. Recommendations for accurate thermal expansion testing are provided.

## INTRODUCTION

Thermal expansion is usually measured by observing the change in length of a uniformly heated rod or bar of material. For many materials, those having a microstructural dimension that is small enough that the material may be viewed as homogeneous on the scale of the specimen rod or bar, the length change in the test is a direct measure of the thermal expansion of the bulk material. However, for 3D carbon-carbon composites, the cross-sectional dimension of the yarns is in the order of 1 mm, which is not very small compared to the dimensions of typical specimens. Insofar as the composite's thermal expansion depends on stress interactions among the various yarns and the matrix pockets, and insofar as these stresses are influenced by the presence of free surfaces at the boundaries of the specimen, the specimen's change in length is not necessarily a direct measure of the thermal expansion of the bulk composite.

The analysis presented in this paper is intended to model stress transfer between constituents of a 3D composite near free surfaces and its effects on the length changes that would be measured in a thermal expansion test. The inputs to the analysis include the thermo-elastic properties of the mini-constituents, as the yarn bundles and matrix pockets are sometimes called, the strength of the interface between a yarn and the rest of the composite, the dimensions of the composite's unit cell, and the length of the specimen. Outputs include the change in specimen length on heating, as a function of how it is measured, and the stresses generated by heating within the yarn and the surrounding composite. Recommendations for avoiding large errors in estimating thermal expansion of the composite can be derived from the results.

## SHEAR LAG ANALYSIS

As shown in Figure 1, the 3D composite is considered to consist of two phases: "yarn", comprising the primary bundles that are oriented axially (normal to the free surface), and "matrix" comprising the other yarn bundles and the matrix pockets. When the composite is heated, differences in the thermal expansions of the two phases give rise to stresses. Generally, on heating of carbon-carbons, the yarn will be in axial tension while the matrix will be in axial compression; perpendicular to the axis, in the transverse direction, the yarn will be in compression (Ref. 1 and 2, for example). At the free surface, in the absence of externally applied tractions, the stresses in yarn and matrix will be zero. Thus, there is a region near the surface in which the stresses vary, which implies the existence of shear at the interface between yarn and matrix. The analysis

Prepared for presentation to the Sixth Rocket Nozzle Technology Meeting of the JANNAF RNTS, Huntsville, 6 December 1984.

Based on research sponsored by the Office of Naval Research under Contract N00014-82-C-0405.

Distribution unlimited; approved for public release.

## TOP VIEW

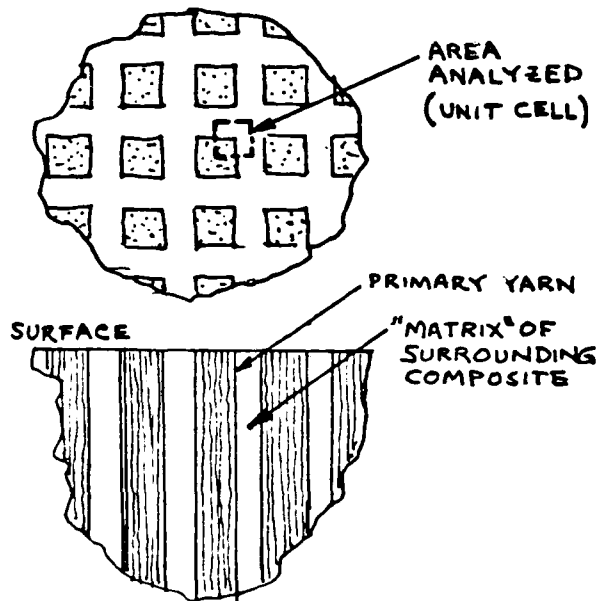


Fig. 1. Idealization of 3D composite.

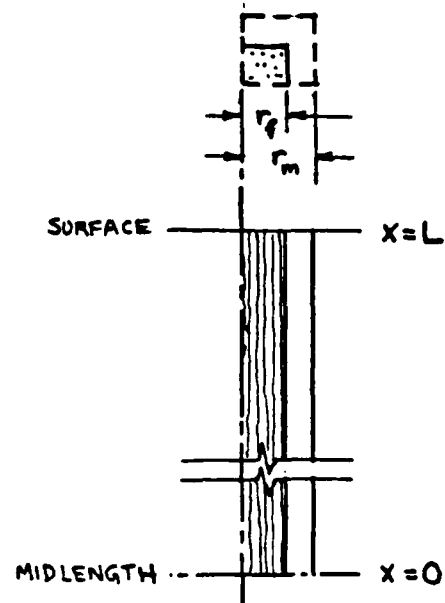


Fig. 2. Unit cell of specimen.

described below defines the stress gradients in terms of a simple shear lag model (adapted from Ref. 3). Once the stresses are defined, the strains and displacements can be calculated for yarn and matrix.

Specifically, we consider simple rectangular bars such as are commonly used for thermal expansion measurements. The symmetry of the situation allows us to do the analysis by studying half the length of such a specimen, considering a single yarn and its surrounding matrix (Fig. 2). Because of the shear lag, the matrix will displace axially more than the yarn, giving rise to a wavy surface at the specimen end. This "roughening" of the surface can produce discrepancies between the measured growth of a specimen and the true thermal expansion of the composite (eg, Ref. 4).

If the interfacial shear stress exceeds the strength of the interface, debonding will occur. In the debonded region, a frictional shear stress can exist, which depends in magnitude on the compressive stress across the interface, among other factors. In the region that remains bonded, the shear stress is predicted from the elastic shear lag analysis. Figures 3 shows schematically the expected relative displacements of yarn and matrix, in the bonded and debonded regions.

We assume the yarns have square cross-sections; it would not be difficult to extend the analysis to rectangular-section yarn bundles, but the major points to be made in this paper can be illustrated with the simpler analysis of square-section reinforcements. Many of the equations for circular-section reinforcements are identical to those for square-section yarns; thus, much of the analysis is also applicable to shear lag between circular fibers and matrix within a yarn bundle.

## Shear Lag Equations

For a specimen that is uniformly heated without any external forces, stress equilibrium requires the axial forces in yarn and matrix to sum to zero at every axial location:

$$\sigma_f r_f^2 + \sigma_m (r_m^2 - r_f^2) = 0 \quad (1)$$

We assume, in accordance with the level of this analysis, that  $\sigma_f$  and  $\sigma_m$  do not vary with radial position.

Consideration of equilibrium, between shear stress and axial stress in the fiber, gives:

$$\tau_f = -\frac{1}{2} r \frac{d\sigma_f}{dx}, \quad r \leq r_f \quad (2)$$

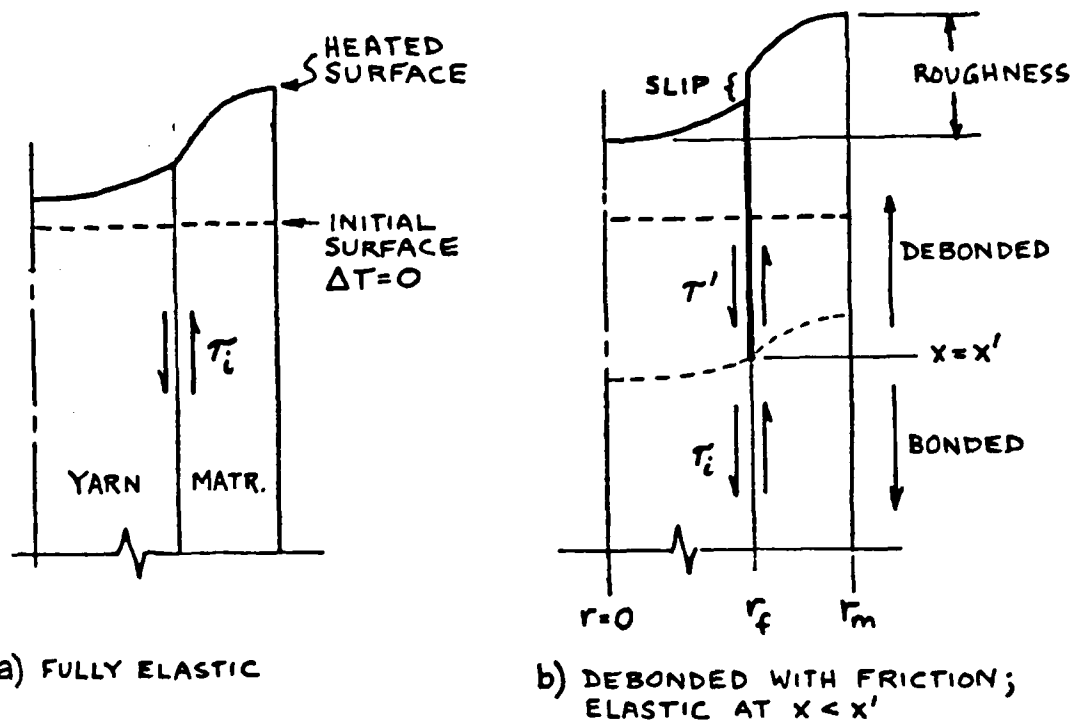


Fig. 3. Schematic of deformations at the free surface.

For the matrix, equilibrium requires:

$$\tau_m = \frac{r_m^2 - r^2}{2r} \frac{d\sigma_m}{dx}, \quad r_f \leq r \leq r_m \quad (3)$$

or, applying Eq. 1 and introducing the yarn volume fraction,  $S^2$ :

$$\tau_m = -\frac{r_m^2 - r^2}{2r} \left( \frac{S^2}{1-S^2} \right) \frac{d\sigma_f}{dx} \quad (4)$$

The shear stress reaches a maximum, for each axial location, at the interface:

$$\tau_i = -\frac{r_f}{2} \frac{d\sigma_f}{dx} \quad (5)$$

When the interface is intact, and the yarn and matrix behave elastically, we may define an average shear strain:

$$\bar{\gamma} = \frac{u_m - u_f}{r_m} \quad (6)$$

which can be related by Hooke's law, to the interface shear stress:

$$\tau_i = G \bar{\gamma} \quad (7)$$

Here,  $G$  is an "effective" shear modulus that represents the fiber and matrix in appropriate proportions and accounts for our use of maximum shear stress in combination with average shear strain. This effective shear modulus may be derived by expressing the average shear strain at given axial location in terms of the average shear strains in yarn and matrix:

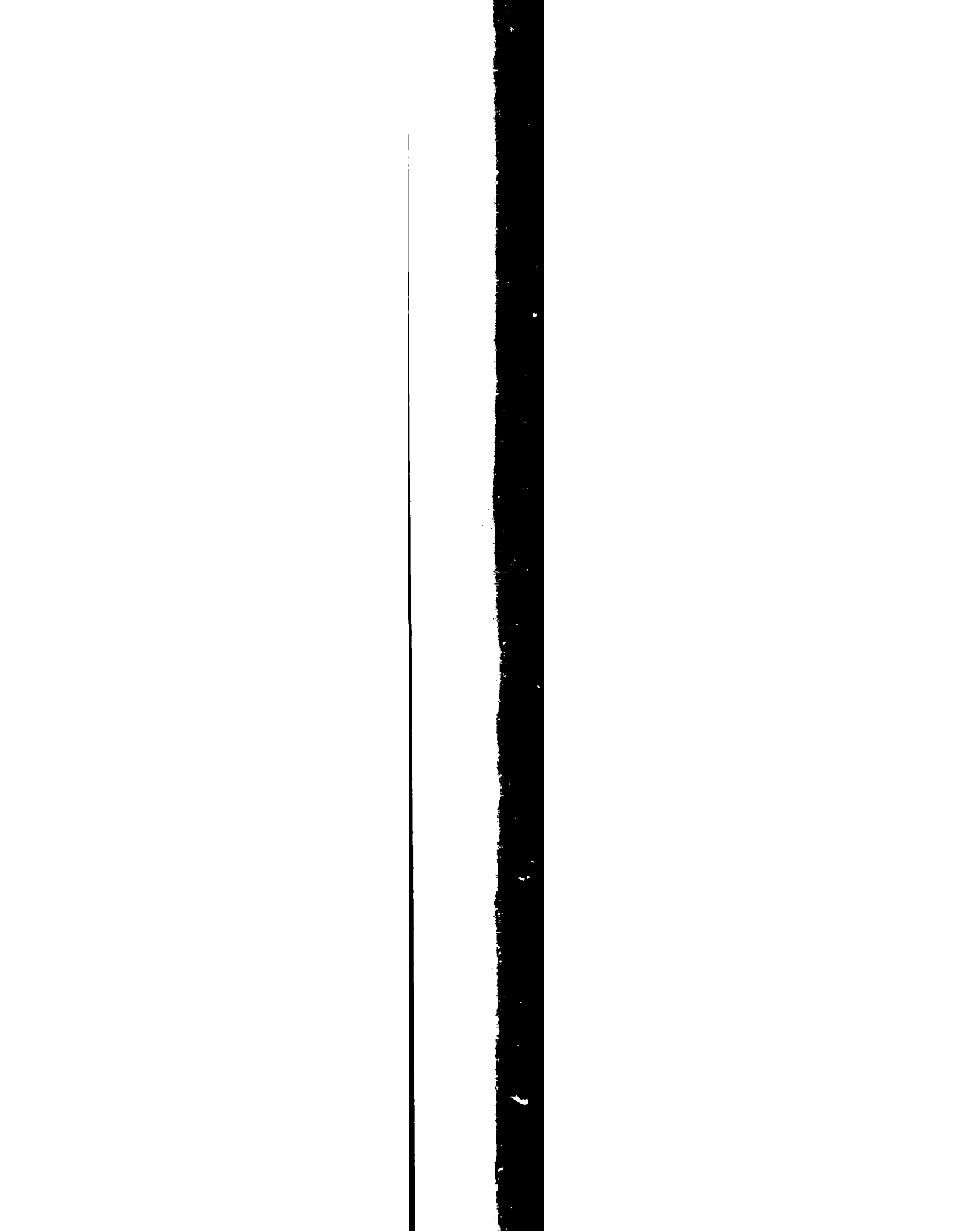
$$\bar{\gamma} = \bar{\gamma}_f S + \bar{\gamma}_m (1-S) \quad (8)$$

Applying Hooke's law:

$$\bar{\gamma}_f = \frac{\bar{\tau}_f}{G_f} \quad \text{and} \quad \bar{\gamma}_m = \frac{\bar{\tau}_m}{G_m} \quad (9)$$

where the average shear stresses are:

$$\bar{\tau}_f = \frac{1}{r_f} \int_0^{r_f} \tau_f dr \quad (10)$$



and

$$\frac{d\tau_i}{dx} = \eta A \cosh(\eta x) \quad (25)$$

For a specimen of finite length, the gradient  $\frac{d\tau_i}{dx}$  at midlength will not, in general, be zero. Thus, the actual maximum yarn stress (at  $x = 0$ ) can be expressed as:

$$\sigma_{f_0} = \phi_0 \sigma_f^* \quad , \quad \phi_0 < 1 \quad (26)$$

Equating Eq 25 and 17, at  $x = 0$ , and using Eq 26, we get a definition of A:

$$A = \frac{1}{\eta} \left. \frac{d\tau_i}{dx} \right|_{x=0} = \frac{G}{\eta r_m} (\alpha_m - \alpha_f) \Delta T (1 - \phi_0) \quad (27)$$

At this point,  $\phi_0$  is undefined. To proceed, we return to consideration of the axial stress in the yarn. From Eq 5 and 26:

$$\sigma_f - \phi_0 \sigma_f^* = -\frac{2}{r_f} \int_0^x \tau_i dx \quad (28)$$

Introducing Eq 24 and integrating:

$$\sigma_f = \phi_0 \sigma_f^* - \frac{2A}{\eta r_f} [\cosh(\eta x) - 1] \quad (29)$$

The yarn axial stress  $\sigma_f'$  at the end of the elastic region ( $x = x'$ ) may be estimated and used in Eq 29 to provide a second relation between A and  $\phi_0$ :

$$A = \frac{(\phi_0 \sigma_f^* - \sigma_f') \eta r_f}{2(\cosh(\eta x') - 1)} \quad (30)$$

If no debonding occurs in the specimen, and it behaves elastically over its entire length, the fiber stress at the end of the elastic region ( $x = L$ ) is zero. If debonding does occur, the fiber stress at the end of the bonded region ( $x = x' < L$ ) is given by Eq 41 (derived in the next Subsection).

We solve for  $\phi_0$  by equating Eq 27 and Eq 30:

$$\phi_0 = \frac{\sigma_f' - 1}{\sigma_f^*} \operatorname{sech}(\eta x') + 1 \quad (31)$$

In this analysis, we solve for  $x'$  numerically by requiring that the shear stress at  $x'$  be the interfacial shear strength. An iterative procedure first assumes an arbitrary value of  $x'$ , solves for  $\phi_0$  and A, computes the elastic shear stress at  $x'$  from Eq 24, and if that value does not equal the shear strength (from Eq 49, below), assumes a new value of  $x'$  and repeats the calculation and so on until the discrepancy is negligible (less than one percent of the shear strength).

The change in length of the matrix, in the bonded region, is:

$$\Delta u_m = \int_0^{x'} \epsilon_m dx = x' \alpha_m \Delta T + \int_0^{x'} \frac{\sigma_m}{E_m} dx \quad (32)$$

Introducing Eq 1 and 29, and performing the integration, we get:

$$\Delta u_m = x' \alpha_m \Delta T + \frac{s^2}{E_m(1-s^2)} \left[ x' \left( \phi_0 \sigma_f^* + \frac{2A}{\eta r_f} \right) - \frac{2A}{\eta^2 r_f} \sinh(\eta x') \right] \quad (33)$$

The corresponding length change of yarn, in the bonded region, may, with the aid of Eq 6, be estimated as:

$$\Delta u_f = \Delta u_m - r_m \bar{\epsilon} = \Delta u_m - \frac{r_m A \sinh(\eta x')}{G} \quad (34)$$

#### Frictional Shear Stress

If the elastic shear stress at the primary yarn interface exceeds the interface shear strength, debonding will occur and the yarn may slip relative to the matrix. A frictional shear stress will exist at the interface. We assume this frictional shear stress  $\tau'$  is the sum of two factors, the product of a friction coefficient  $\mu$  and the compressive stress  $\sigma_c$  acting across the interface, and a constant  $\tau^*$  representing resistance by other effects, such as mechanical interlocking between rough interface surfaces:

$$\tau' = \tau^* - \mu \sigma_c \quad (35)$$

The transverse compressive stress arises from the minimechanical interactions between the transverse yarns and the rest of the composite (which includes our primary axial yarn). Because shear lag phenomena apply also to the transverse yarns, the compression will vary with distance from a

transverse free surface. At a transverse surface, the compressive stress on the primary yarn will approach zero. Toward the center of a large enough body, the compressive stress will approach a maximum value  $\sigma_c^*$  that, for each set of transverse yarns may be estimated as (eg, Ref 2):

$$j\sigma_c^* = E_{fT} (\bar{\alpha}_j - \alpha_{fT}) \Delta T \quad (36)$$

where  $\bar{\alpha}_j$  is the composite's thermal expansion:

$$\bar{\alpha}_j = \frac{\alpha_f E_f v_j + \alpha_m E_m (1 - v_j)}{E_f v_j + E_m (1 - v_j)} \quad (37)$$

and  $v_j$  is the yarn volume fraction in the appropriate direction. For illustrative purposes, we simplify the analysis to deal only with square primary yarns in a matrix characterized by equal distribution of yarns in the two transverse directions. Then:

$$\sigma_c^* = E_{fT} \Delta T \left( \frac{\alpha_f E_f v_T + \alpha_m E_m (1 - v_T)}{E_f v_T + E_m (1 - v_T)} \right) \quad (38)$$

where

$$v_T = \frac{v_T - S^2}{2} \quad (39)$$

and  $v_T$  is the total volume fraction of yarn in the composite, usually in the vicinity of .7 to .75. The task of estimating the compressive stress distribution in a slender bar specimen is not trivial as it would require iterative application of the shear lag analysis to the primary and transverse yarns. To illustrate the effects, we define a factor  $\psi$ :

$$\sigma_c = \psi \sigma_c^* , \quad \psi \leq 1 \quad (40)$$

and we consider two examples in the application of the analysis: 1)  $\psi = 0.1$  as applying approximately to the corners of a specimen, and 2)  $\psi = 1.0$  (maximum compression) as providing a bound to the situation at the specimen centerline (Figure 4).

We assume further that the frictional shear stress is invariant with axial position. Then, by integrating Eq. 5, we find the distribution of axial stress in the yarn to be:

$$(41) \quad \sigma_f = \frac{2\tau'}{r_f} (L - x) , \quad x \geq x'$$

The change in length of the yarn in the debonded region is:

$$(42) \quad f_r u_f = \int_{x'}^L e_f dx$$

and the length change of matrix is:

$$(43) \quad f_r u_m = \int_{x'}^L e_m dx$$

Performing the integrations, we get:

$$(44) \quad f_r u_f = \alpha_f \Delta T (L - x') + \frac{\tau'}{r_f E_f} (L - x')^2$$

and

$$(45) \quad f_r u_m = \alpha_m \Delta T (L - x') - \frac{\tau'}{r_f E_m} \left( \frac{S^2}{1 - S^2} \right) (L - x')^2$$

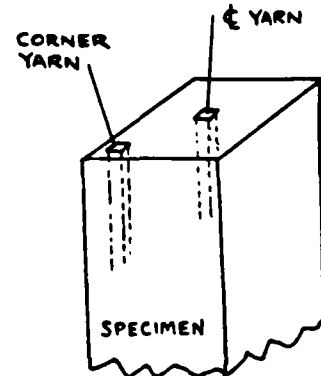


Fig. 4. Yarn positions.

#### Total Length Change of the Specimen on Heating

From Eq 44 and 45, and Eq 33 and 34, it is clear that the length change measured in a thermal expansion test will depend on whether the test technique reads the length change of the matrix or of the yarn. The total length change of the matrix region is the sum of the length changes in the bonded and debonded regions:

$$u_m^* = e_l u_m + f_r u_m \quad (46)$$

Similarly, the total length change of the yarn is:

$$u_f^* = e_l u_f + f_r u_f \quad (47)$$

The difference between these two length changes is the surface roughening shown in Figure 3.

## INPUT PROPERTIES

The illustrative results presented later are intended to represent graphitized 3D carbon-carbon material made with T-300 yarns with pitch densification, such as used in the 7-inch and 15-inch billet programs (Ref. 5 and 6). This section describes the approach to estimating the material properties used in the analysis. The values used to produce the illustrative results (next Section) are listed in Table 1.

The axial modulus and thermal expansion of the yarn phase are derived from test data. For modulus, the correlation by F. I. Clayton, reported in Ref. 6, provides estimates of in-situ filament modulus  $E_{fil}$  vs. temperature. We assume the yarn is composed of 60 percent filament by volume, so that  $E_f \approx .6 \times E_{fil}$ . For axial thermal expansion of the yarn, we use directly the data obtained by Lander (Ref. 7) on a specimen comprising a single yarn bundle.

The transverse expansion of the matrix phase (that includes the transverse yarns and matrix pockets) is based directly on the measurements by Lander (Ref. 7) on a specimen from which the axial yarns were excised.

The remaining properties of the matrix phase and of the yarn are estimated using simple rule-of-mixtures equations from values for filaments and pitch-precursor matrix recommended by Kibler (eg, Ref. 8). Estimates are required here because direct experimental data are unavailable.

Graphitized 3D carbon-carbons are known to have a regularly cracked microstructure (Ref. 2, for example). In the current context, the existence of these microcracks affects the thermo-elastic properties of the matrix region, the transverse elastic properties of the yarn, and the effective shear modulus used in the shear lag analysis. The simplest approach to accounting for the microcracks is to assign efficiency factors to the extensional and shear moduli of the matrix material (eg, Ref. 8 and 9):

$$\eta_E = \frac{E_m}{E_m^*} = \frac{E_{ET}}{E_{ET}^*} \quad \eta_S = \frac{G_m}{G_m^*} = \frac{G_f}{G_f^*} \quad (48)$$

where the "starred" properties represent uncracked material. Following the recommendation of Ref. 9, we assign a lower efficiency to the extensional behavior than to the shear behavior. From Kibler's work, we use a shear efficiency factor of 0.4. From attempts to match some of Lander's thermal expansion data (Ref. 7), it appears that the extensional efficiency factor is in the vicinity of .05 to .10.

Data for interfacial shear strength and friction coefficients is lacking. From a brief review of related information (eg, pull-out failures in tensile tests, microshear data, shear tests of 1D and 2D composites, and friction coefficients measured at room temperature between composite parts) approximate values were estimated. The values used in the illustrative calculations are listed in Table 1.

The input value for shear strength,  $\tau_{EL}^*$ , represents the strength in the absence of substantial compression across the interface. For high values of  $\alpha_c$  it is possible that the estimated friction shear stress (Eq 35) will be greater than the input shear strength. While other approaches are also attractive (eg, use of a multiaxial fracture criterion for shear strength), in this paper we take the effective elastic shear strength,  $\tau_{EL}$ , to be the larger of the input strength and the estimated friction shear stress:

$$\tau_{EL} = \text{MAX} [\tau_{EL}^*, T'] \quad (49)$$

TABLE 1. INPUTS TO ILLUSTRATIVE ANALYSIS

PROPERTY	VALUE AT TEMPERATURE						
	Temp, F	0	1000	2000	3000	4000	
shear modulus, yarn	psi	$G_f^*$	1.50E+06	1.51E+06	1.60E+06	1.71E+06	1.49E+06
shear mod, transverse composite	psi	$G_m^*$	5.36E+05	5.43E+05	5.75E+05	6.12E+05	5.34E+05
Young's modulus, yarn, axial	psi	$E_f$	3.60E+07	3.60E+07	3.60E+07	2.40E+07	2.10E+07
Young's modulus, yarn, transverse	psi	$E_{fT}^*$	1.38E+06	1.41E+06	1.50E+06	1.61E+06	1.42E+06
Young's modulus, transv. composite	psi	$E_m^*$	1.38E+06	1.41E+06	1.50E+06	1.61E+06	1.42E+06
extensional bond efficiency		etaE	0.05	0.05	0.05	0.05	0.05
shear bond efficiency		etaS	0.40	0.40	0.40	0.40	0.40
CTE, yarn, axial	per F	alpF	0.00E+00	-2.00E-07	2.00E-07	4.00E-07	5.50E-07
CTE, yarn, transverse	per F	alpFT	0.00E+00	4.64E-06	4.46E-06	4.33E-06	4.89E-06
CTE, transverse composite	per F	alpm	0.00E+00	1.60E-06	2.25E-06	3.00E-06	3.75E-06
nominal interface shear strength	psi	tauEL*	1000	1000	1000	1000	1000
minimum frictional shear strength	psi	tau'	200	200	200	200	200
coeff. friction		mu	0.3	0.3	0.3	0.3	0.3
total yarn volume fraction		vY	0.75	0.750	0.750	0.750	0.750

## ILLUSTRATIVE RESULTS

The shear lag analysis is applied here to the prediction of thermal expansion data as a function of the technique used for measurement of specimen length change. The various specimen configurations and length measurements used for 3D carbon-carbons are sketched in Figure 5.

The first example deals with analysis of "matrix" expansion  $u_m^*$  and yarn expansion  $u_y^*$ , providing calculations that may be compared to Lander's data (Ref. 7) for flat-ended and protruding-yarn specimens, respectively. Lander tested 2-inch long specimens taken from the outer-diameter region of a woven cylindrical billet, oriented in the billet's axial direction. We used the input properties shown in Table 1 and implemented the analysis using an estimated yarn volume fraction of 0.19 and a unit-cell radial dimension,  $r_m$ , of .07 inch. Figure 6 shows the analytical predictions to be in reasonable agreement with Lander's data up to about 2200 C (4000 F). Correlations above 4000 F were not attempted because the analysis does not currently include creep/relaxation effects, which are important at higher temperatures.

The predictions are shown as lines in Figure 6; the top solid line is the prediction for the corner of a flat specimen where the frictional stress is reduced because minimal compression can exist across the yarn interface; the bottom solid line is the prediction for the centerline region of a flat specimen that is sufficiently large in cross-section to exhibit maximum compression at the yarn interface. The lines tend to bracket Lander's data, suggesting that the analytical model is capable of predicting the major effects in such specimens. Also shown is the predicted response of the yarn, which corresponds to data from protruding-yarn specimens. The difference between predicted responses of yarns at the corner and centerline is negligible, so only one dotted line is plotted. In Figure 7, these predictions are compared to the theoretical response of the bulk composite (estimated by Eq 37); we see that the yarn responses are quite close to the theoretical value, whereas the matrix response is a substantial overestimate.

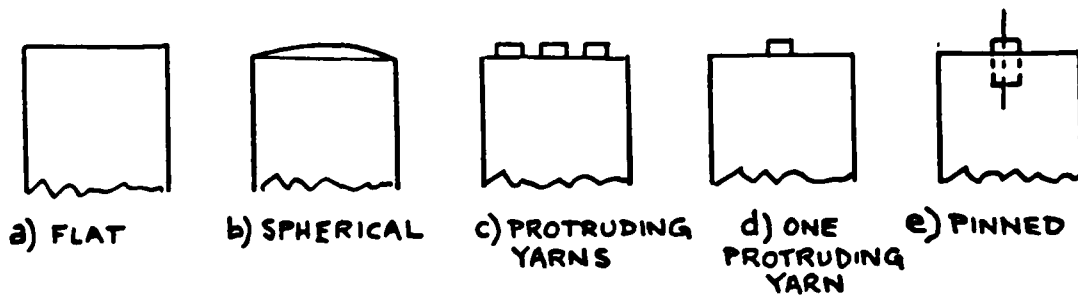


Fig. 5. Various end configurations used in thermal expansion testing.

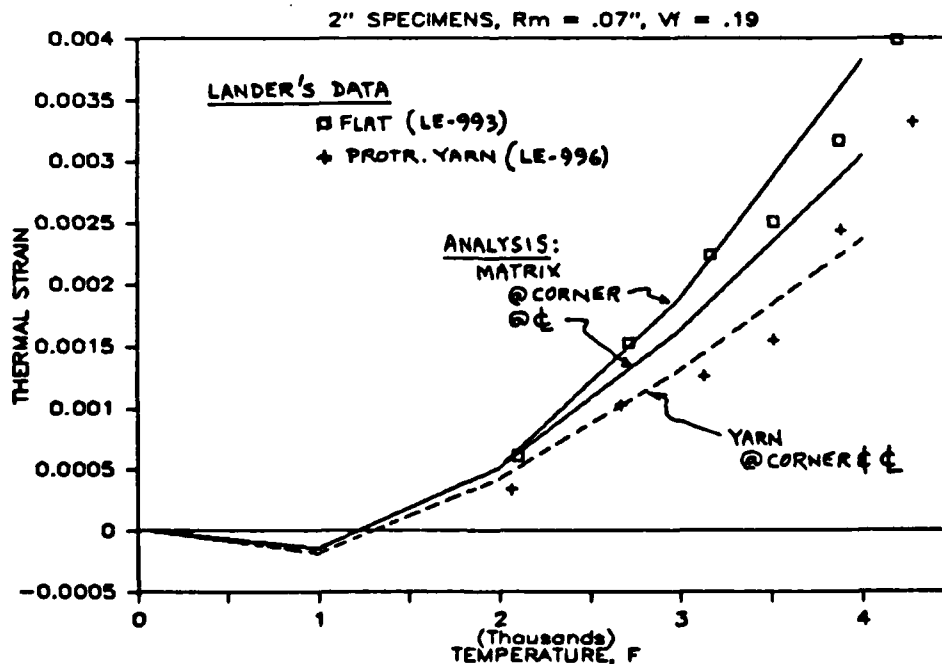


Fig. 6. Comparison of analysis to Lander's data for flat and protruding-yarn specimens.



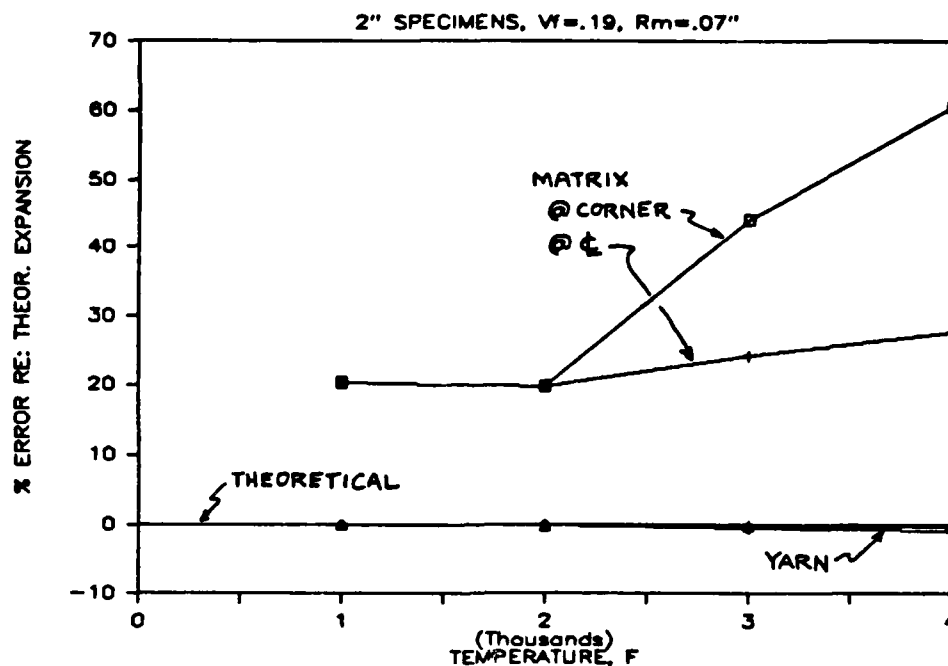


Fig. 7. Discrepancies between predicted measurements and theoretical expansion of bulk composite.

Figure 8 shows the predicted roughening (in hundredths of an inch) of a flat end-surface and the predicted extent of debonding. Figure 9 shows the predicted variation of yarn axial stress and interface shear stress, for the centerline region.

Additional analyses were done to explore the effects of specimen length (actually, the key variable is the ratio of specimen length to unit-cell dimension,  $r_m$ ) and yarn volume fraction. For these calculations, we assumed the yarn experiences the maximum transverse compression. Thus the data provide a low-bound expansion for the centerline of flat-ended or spherical-ended specimens. Also, the interface shear strength was taken as 2000 psi, rather than the 1000 psi used in analyzing Lander's data.

The effect of specimen length on predicted expansion data to 4000 F is shown in Figure 10, for a yarn fraction of .21 and a unit-cell radius of .07-inch. We see that the potential errors from using flat-ended specimens decrease as specimen length increases. It may be of interest to note that the specimen lengths used for expansion measurements on fine-weave carbon-carbons (eg, Ref. 10) were sufficient to make such errors nearly negligible; to achieve similar accuracy with the coarse weave composites such as the billet Lander studied, we would need specimen lengths in the order of ten inches. The predicted surface roughening and the length of debond are insensitive to specimen length, in the range studied. The yarn stress generated at the specimen midlength is within one percent of the theoretical value, even for the shortest length shown; this is consistent with the length of the shear-lag region shown in Fig 9. Thus, the assumption of full compression across the centerline yarn interface may be close to reality for specimens about 3/8-inch in cross-section. However, as noted earlier, the proper analysis of the transverse compression is complex, so the implication just stated should be viewed cautiously.

The effects of yarn volume fraction on predicted expansion data to 4000 F are shown in Figure 11, for 2-inch long specimens having a unit-cell radius of .07 inch. Potential errors in the use of flat-ended specimens increase significantly at low values of yarn volume fraction. This finding may aid in explaining some of the very high values of radial-direction expansion reported for some cylindrical billet materials (eg, Ref. 6).

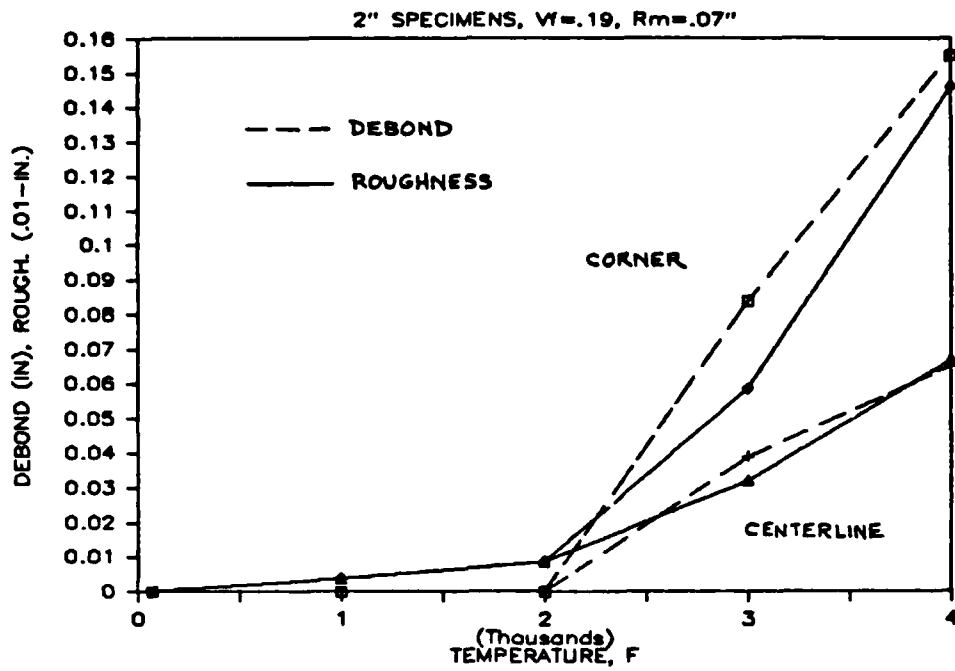


Fig. 8. Predicted extent of debonding and surface roughening at 4000 F in specimens of Fig. 6.

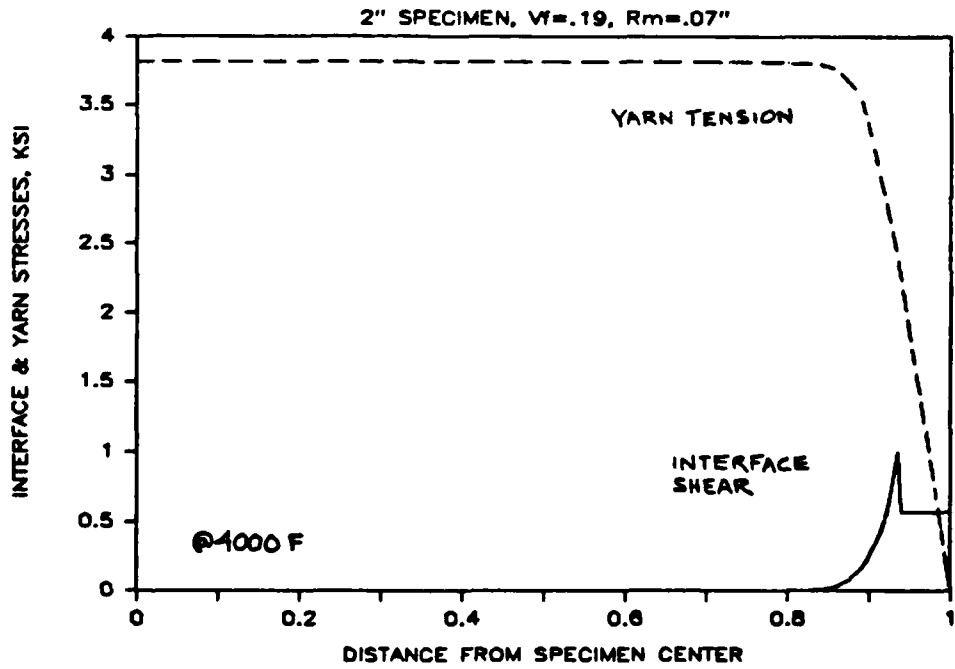


Fig. 9. Predicted stress gradients at interface and in yarn at 4000 F at specimen centerline.

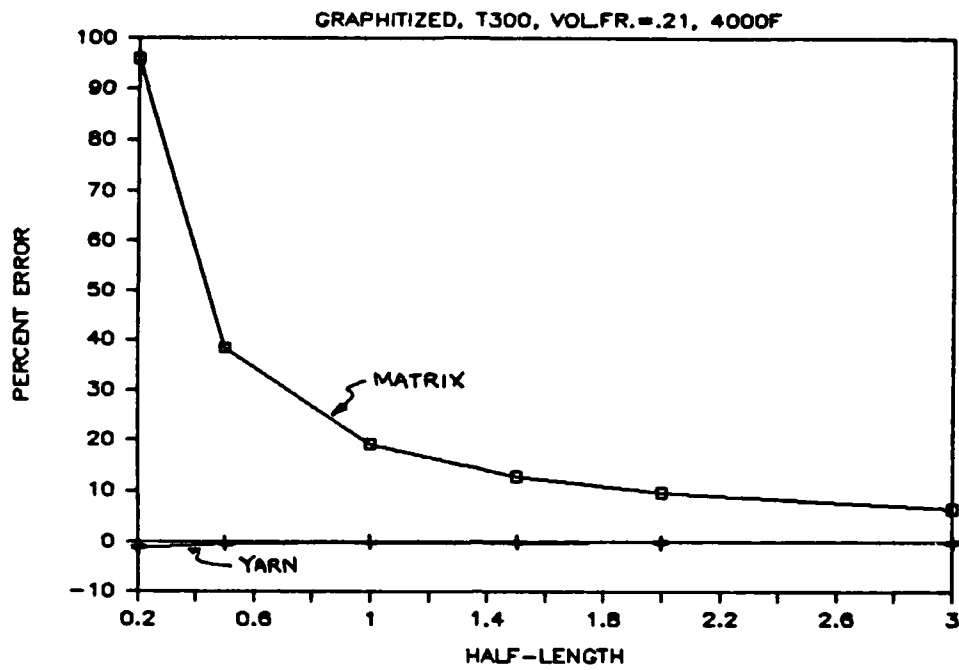


Fig. 10. Effect of specimen half-length on predicted errors at 4000 F.

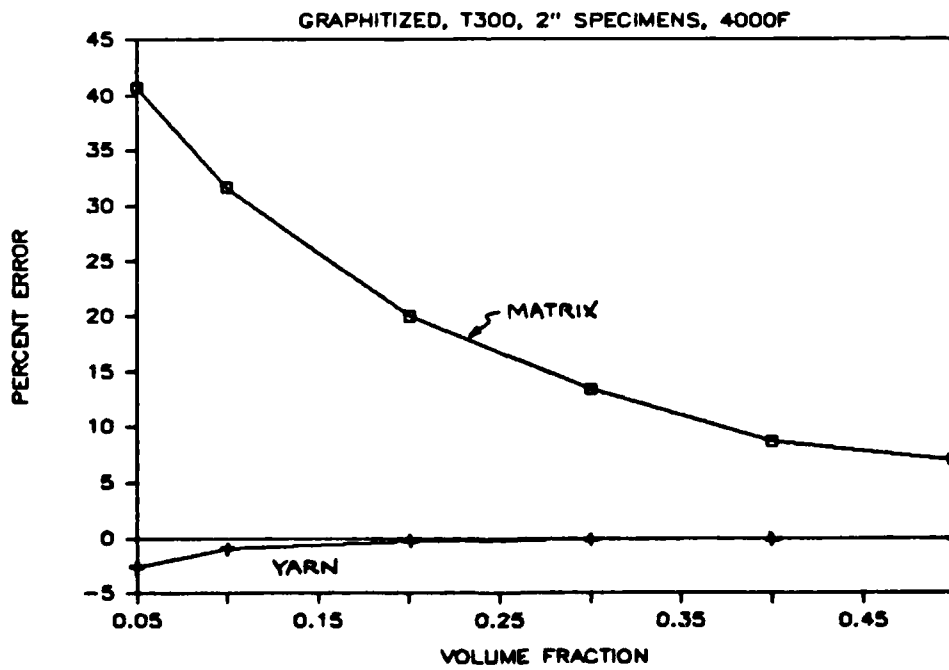


Fig. 11. Effect of yarn volume fraction on predicted errors at 4000 F.

## CONCLUDING REMARKS

The shear lag analysis shows that thermal expansion data can be sensitive to the details of the measurement technique, especially to the length of specimen used and to the manner of measuring its change in length (Figure 5). Potential errors are larger for specimens of smaller volume fraction of yarns in the direction of measurement, and for coarse-weave composites.

On the basis of the findings, the use of flat-ended specimens should be discouraged. The use of spherical-end specimens is preferable to flat-end specimens; however, significant error may be experienced due to surface roughening. The use of pin-ended specimens should provide quite accurate data if the pin rests on the end of a yarn and is of a diameter smaller than the yarn cross-section; otherwise, data from pinned specimens may be influenced by roughening at the base of the pin. (The shear lag analysis could readily be extended to treat the effect of pin depth). Of all the configurations shown in Figure 5, the most accurate appears to be the protruding-yarn specimen (Fig. 5c) which was first used by Lander in the end-effects study of Ref. 7.

Many of the properties that are inputs to the analysis are not well known. It is recommended that research be directed toward measuring transverse properties of yarn bundles, in-situ properties of matrix-pocket regions, establishing the appropriate efficiency factors to account for pre-existing microcracks, measuring yarn interface strengths and friction coefficients, all as functions of temperature. While some data of the types listed is available, more is needed for specific materials of interest.

It would be worthwhile to attempt experimental verification of the predicted debond lengths and surface roughenings.

Currently, the analysis does not treat creep/relaxation effects, which are undoubtedly important at temperatures above 4000 F. Extension of the analysis, and the acquisition of relevant constituent creep data would be worthwhile. Other extensions of the analysis should also be attempted. These include treatment of rectangular-section yarns, allowance for differing volume fractions for the two sets of transverse yarns, and better treatment of the compressive stresses that influence the frictional shear.

Motivation for the suggested further work includes the belief that shear lag analysis is a powerful tool for studying the structural response of 3D carbon-carbon components near free surfaces. In comparison to finite-element analyses of mini-mechanical interactions, the shear lag approach is simple and inexpensive; the simplifications (including neglect of Poisson's interactions) and lack of rigor (in the sense of elasticity solutions) are compensated for by the ability to treat approximately such phenomena as inter-constituent slip, which are difficult to model rigorously.

## NOMENCLATURE

$\alpha$  = thermal expansion coefficient, secant value

$\gamma$  = shear strain

$\sigma$  = extensional stress

$\tau$  = shear stress

E = Young's modulus

G = shear modulus

L = half the length of the specimen

S = ratio of yarn radius to matrix radius

T = temperature

e = extensional strain, total

r = radial distance, or radius

u = axial displacement

v = volume fraction of yarn

x = axial distance

## Subscripts

c = compression

f = pertaining to yarn

i = pertaining to interface

j = index defining a yarn direction

m = pertaining to matrix

T = transverse to the yarn axis

## ACKNOWLEDGMENTS

Support of this research by the Office of Naval Research and the encouragement offered by Dr. L. H. Peebles, Jr., ONR's Scientific Officer, are gratefully acknowledged. The author also thanks Mr. Louis L. Lander, of FMI, for valuable discussions of thermal expansion measurement techniques and data interpretation, and for early access to his experimental data.

## REFERENCES

1. Greszczuk, L. B., "Analysis of Dimensional Changes and Fiber-Matrix Interactions During Processing of 3D Carbon-Carbon Composites", Extended Abstracts 13th Biennial Conference on Carbon, American Carbon Society, 1977, pp70-71.
2. Jortner, J., Thermal Expansion and Bimodularity of 3D Carbon-Carbon Composites, Annual Report to ONR, Contract N00014-80-C-0717, November 1981.
3. Rosen, B. W., Mechanics of Composite Strengthening, presented at ASM Seminar on Fiber Composite Materials, October 1964.
4. Jortner, J., and Clayton, F. I., "Effects of Free-Surface Roughening on Thermal Expansion Data", JANNAF Rocket Nozzle Materials Report, Vol.1, No.5, August 1979.
5. Ellis, R. A., and Kearney, W. J., Cylindrical Carbon-Carbon ITE (7-in. Billet Program), AFRPL-TR-83-057, November 1983.
6. Ellis, R. A., 3D Carbon-Carbon Billets (15-in. Billet Program), AFRPL-TR-82-042, July 1982.
7. Lander, L. L., Final Report on Mechanical and Thermal Properties of Seven-Inch Man-Tech Billet Program, FMI Report EMTL-MT-83-1592, March 1983. (see Appendix C).
8. Kibler, J. J., et al, Exploratory Development of In-Process Yarn Bundle Properties, AFWAL-TR-80-4096, July 1980. See also Kibler and Chatterjee, Development of a Mini-Mechanics Model for 3-D Carbon-Carbon Composites, MSC Report TFR 7510, 1975.
9. Jortner, J., Thermal and Mechanical Behavior of Carbon-Carbon Composites, Annual Report to ONR, Contract N00014-82-C-0405, January 1984.
10. Littleton, H. E., and Pears, C. D., Mechanical, Thermal and Nondestructive Characterization of GE-2.2.3, AFML-TR-77-48, April 1977.

## APPENDIX C

## "EFFECTS OF WEAK INTERFACES ON THERMAL EXPANSION OF 3D C-C COMPOSITES"

The following pages are a copy of the extended abstract that is to appear in the Proceedings of the 1985 Carbon Conference, Lexington, Kentucky, June 1985. The content is essentially a condensed version of Appendix B.

PREVIOUS PAGE  
IS BLANK



To be presented at the 17th Biennial Conference on Carbon, University of Kentucky, June 1985.

EFFECTS OF WEAK INTERFACES ON THERMAL EXPANSION OF 3D CARBON-CARBON COMPOSITES

by

Julius Jortner  
Jortner Research & Engineering, Inc.  
Costa Mesa, California 92628

Interfaces between the constituents of carbon-carbon composites usually are weak. Therefore, transfer of stress from one constituent to another can require relatively long "shear lag" distances because the interface fails and, instead of efficient elastic stress transfer, only friction and mechanical-interlock forces are available. Detrimental effects on tensile strength have been identified (1,2). This paper shows that weak interfaces also affect the measurement of thermal expansion of 3D carbon-carbons.

Thermal expansion usually is measured by observing the change in length of a uniformly heated bar. For materials of a microstructural dimension small enough to be considered homogeneous on the scale of the specimen, the length change is a direct measure of the thermal expansion of the bulk material. However, for 3D composites, the diametral dimension of the yarns is in the order of  $\mu\text{m}$ , which is not very small compared to typical specimens. As the composite's thermal expansion depends on stress interactions among the variously oriented yarns, and as these stresses are affected by free surfaces at the boundaries of the specimen, the change in length is not necessarily a direct measure of the thermal expansion of the bulk composite.

For this analysis, the 3D composite is taken to consist of two phases: "yarn", comprising the primary bundles that are oriented axially (parallel to the bar's length), and "matrix" comprising the other yarn bundles and the matrix prelets. Differences in the thermal expansions of the two phases give rise to stresses when the bar is heated. Generally, the "yarn" will be in axial tension while the "matrix" will be in axial compression; transverse to the axis, the interface will be in compression (3). At the end of the bar, in the absence of externally applied forces, the axial stresses in yarn and matrix will be zero. Thus, near the end, the axial stresses vary, implying shear at the yarn-matrix interface.

Specifically, we consider simple square bars as are commonly used. The symmetry of the situation allows us to study half the length of such a specimen, considering a single yarn and its surrounding matrix (Fig. 1). Because of shear lag, the matrix will displace axially more than the yarn, giving rise to a wavy surface at the specimen end (Fig. 1). In the region that remains bonded, the shear stress can be predicted from an elastic shear lag analysis. If the interface shear stress exceeds the interface strength, debonding will occur. In the debonded region, a frictional shear stress can exist, which we assume

is the sum of two factors: the product of a friction coefficient  $\mu$  and the transverse compressive stress  $\sigma_c$  acting across the interface, and a constant  $\tau'$  representing resistance by other effects, such as mechanical interlocking between rough interface surfaces. The compressive stress,  $\sigma_c$ , arises from the minimechanical interactions between the transverse yarns and the rest of the composite (which includes our primary axial yarn). Because shear lag phenomena apply also to the transverse yarns, the compression will vary with distance from a transverse free surface. At a transverse surface, the compressive stress on the primary yarn will approach zero. Toward the center of a large enough body, the compressive stress will approach a maximum value. Thus, we may consider two extremes, one applying to the corner of a specimen and the other applying to the centerline (Fig. 2).

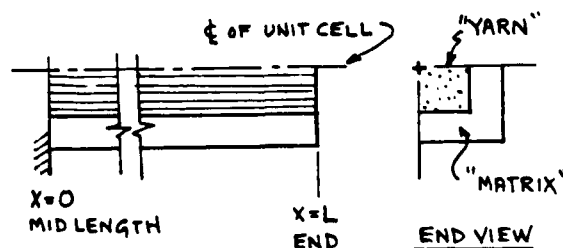


Fig. 1. Idealization of 3D composite for analysis.

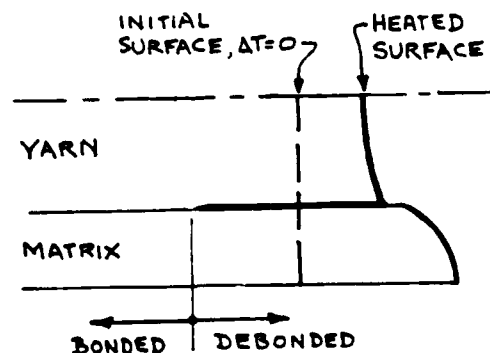


Fig. 2. Deformation of end surface on heating.

From these considerations, it is clear that the thermal strain measured in an expansion test will depend on whether the test technique reads the length change of the "matrix" phase or of the "yarn" phase, and will also depend on whether the measurement includes the corners of the specimen or just the centerline. Thus, various types of specimen ends used in dilatometer tests (Fig. 4) may give different data.

Numerical examples have been calculated, based on input properties intended to represent 3D composites made with T-300 fibers, densified with pitch to more than  $1.8 \text{ g/cm}^3$ , and heat-treated to temperatures above  $2200 \text{ C}$ . Fig. 5 shows the predicted length changes (divided by specimen length) for 50 mm long bars with 21 percent of the volume occupied by axial yarn bundles that are 1.6 mm square. Three curves are shown: (A) "matrix" phase response at corner of specimen, (B) "matrix" phase response at centerline of specimen, and (C) "yarn" phase response at centerline. The predicted yarn response at the corner is essentially the same as (C). The data points are from Lander (4): squares were measured on flat-ended specimens in a way that includes the "matrix" response; crosses were measured on a specimen with protruding yarns, so they represent "yarn" response. There is respectable agreement between data and analysis. Both show that substantial differences can occur between the two types of measurement. Analysis shows that the yarn response is very close to the theoretical expansion of the composite. Therefore, we may conclude that dilatometry on flat-ended specimens can produce substantial overestimates of the true expansion of the composite. Increasing the ratio of specimen length to yarn diameter, and increasing the volume fraction of yarn, will tend to decrease the errors.

On the basis of the findings, the use of flat-ended specimens in dilatometers should be discouraged. The use of spherical-end specimens is preferable to flat-end specimens; however, significant error may be experienced due to surface roughening. Pin-ended specimens should be quite accurate if the pin rests on the end of a yarn and is of a diameter smaller than the yarn cross-section; otherwise, data from pinned specimens may be influenced by roughening at the base of the pin. Of the ends shown in Fig. 4, the most accurate appear to be the protruding-yarn specimens (Fig. 4c/d) first used by Lander (4)

Many of the properties that are inputs to the analysis are not well known. Research should be directed toward measuring transverse properties of yarn bundles, accounting for pre-existing microcracks, and measuring yarn interface strengths and friction coefficients, all as functions of temperature. Also, the analysis now does not treat creep/relaxation effects, which are undoubtably important at temperatures above  $2000 \text{ C}$ ; extension of the analysis, and acquisition of relevant creep data would be worthwhile.

#### Acknowledgments

Sponsored by the Office of Naval Research. Thanks to Mr. L. L. Lander for stimulating discussions.

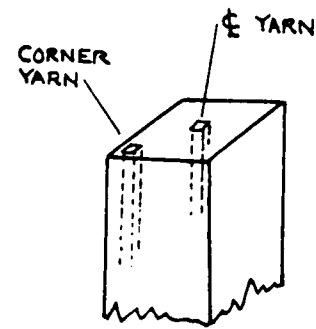


Fig. 3. Extreme yarn positions in specimen.

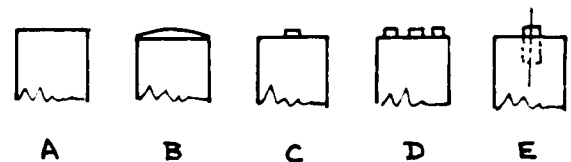


Fig. 4. Various ends for dilatometer specimens: A = flat B = spherical C = protruding yarn D = protruding yarns E = hole with pin

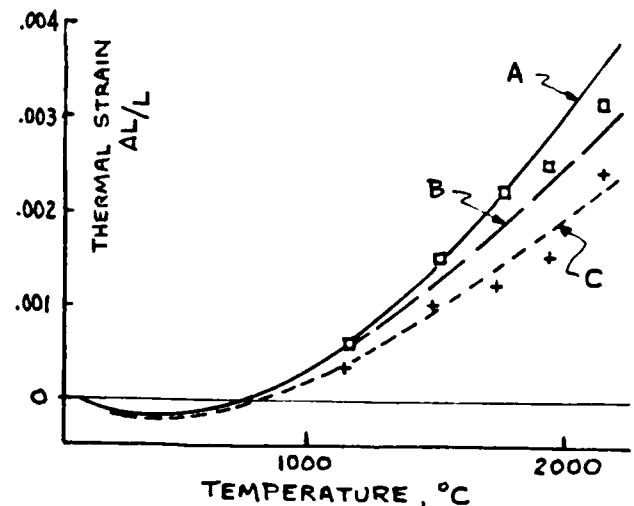


Fig. 5. Effects of end type on thermal strain data: analytical predictions and Lander's data.

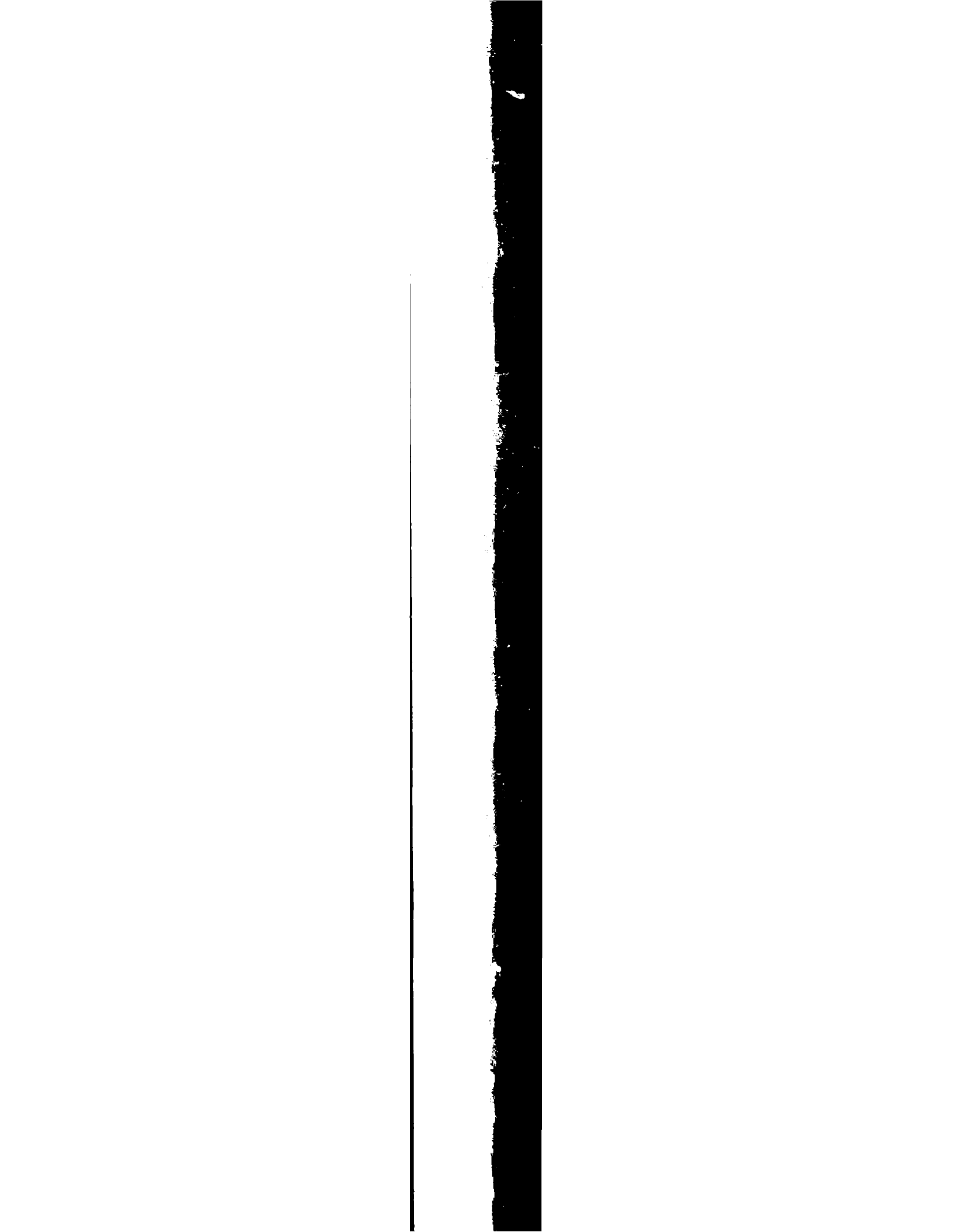
#### References

1. Chatterjee, S. N., et al, Proc. AIAA/ASME JSM Conf., 1976, pp184-192.
2. Jortner, J., A Model for Tensile Fracture of C/C Fiber Bundles, in preparation.
3. Greszczuk, L. B., 13th Carbon Conf. Abstracts, American Carbon Society, 1977, pp70-71.
4. Lander, L. L., Unpublished Data, 1980-81.



## REFERENCES

1. Jortner, J., Thermal Expansion and Bimodularity of 3D Carbon-Carbon Composites, Annual Report to ONR under contract N00014-80-C-0717, November 1981.
2. Jortner, J., Thermal Expansion, Shear Deformation, and Bimodularity of 3D Carbon-Carbon Composites, Final Report to ONR under contract N00014-80-C-0717, April 1982.
3. Jortner, J., Thermal and Mechanical Behavior of Carbon-Carbon Composites, Annual Report to ONR under contract N00014-82-C-0405, January 1984.
4. Peebles, L. H., Jr., (Editor), Proceedings of the ONR Workshop on Research Priorities in Carbon/Carbon Composites, NRL Memorandum Report 5509, December 1984.
5. Jortner, J., Outline of Research Needs for Effects of Material Defects on Thermostructural Performance of Carbon-Carbon Composites in Rocket Nozzles, presented to AFRPL C-C Workshop, El Segundo, 22 May 1984.
6. Jortner, J., A Tensile Strength Model for Filamentary Composites with Weak Interfaces, presented to 37th Pacific Coast Regional Meeting of American Ceramic Society, San Francisco, 29 October 1984.
7. Kibler, J. J., and Chatterjee, S. N., Development of a MiniMechanics Model for 3-D Carbon-Carbon Materials, Materials Sciences Corp Report TFR-7510, 1975.
8. Jortner, J., Effects of Anomalies on Thermostructural Behavior of 3D Carbon-Carbon Composites, AFWAL-TR-82-4118, October 1982.
9. Loomis, W. C., et al, Analytical Processing for Improved Composites (APIC), Vol.II. Analytical Modeling, AFWAL-TR-80-4147 (Vol.II), October 1980. See also AFWAL-TR-81-4082, August 1981, same title.
10. Grose, James G., and Jones, Robert M., SAAS III Finite Element Stress Analysis of Axisymmetric and Plane Solids..., SAMSO-TR-71-103, 22 June 1972.
11. Kibler, John J., et al, Structural Assessment of 3-D Carbon/Carbon Cylinders During Processing, AFML-TR-78-75, April 1978.
12. Jortner, J., et al, Application of Carbon-Carbon Composites to Rocket Nozzles (ACORN) - Interim Report, AFML-TR-78-196, December 1978. (See Section 5).
13. Loomis, W. C., et al, Rocket Nozzle Processing Science (APIC/RN), AFWAL-TR-81-4118, November 1981.



stresses During Fabrication of  
on Composites," Thermomechanical  
posites, J. Jortner, ed., American  
Booklet AD-04, 1982, pp.63-76.

nd Batdorf, S. B., The Effects of  
lly Reinforced Carbon-Carbon  
N.R. under Contract N00014-77-0505,

., Cylindrical Carbon-Carbon ITE  
R-83-057, November 1983.

and Buch, J. D., Annual Status  
bon-Carbon Composites for Solid  
, Aerospace Report No.  
1983.

R., "On the Failure of Billet A9",  
Vol.3, No. 4, October 1981. (see  
80. (see Sections 6.8 and 6.9)

nd Pitch Billet A9, SoRI Special  
1981.

lindrical Carbon-Carbon  
4, August 1980. (see Sections 6.8

ed Experimental Information to  
Strain Relations", Proc. Intl. Conf.  
ng Materials, C. S. Desai and R. H.  
na, Tucson, January 1983.

d data, Lockheed Corporation,

ed Composites Design Guide, 3rd  
Materials, January 1977.

ion to Applied Anisotropic  
ress, 1961.

EI

FI

D

